Int J Earth Sci (Geol Rundsch) (2017) 106:991–1021
DOI 10.1007/s00531-016-1347-7

ORIGINAL PAPER

Processes and controlling factors of polygenetic dolomite formation in the Transdanubian Range, Hungary: a synopsis

János Haas[1] · Kinga Hips[1] · Tamás Budai[2] · Orsolya Győri[1] · Georgina Lukoczki[1,3] · Sándor Kele[4] · Attila Demény[4] · Zsófia Poros[1,5]

Received: 8 December 2015 / Accepted: 25 May 2016 / Published online: 16 June 2016

Abstract In the Transdanubian Range (Hungary), dolostone and dolomitic limestone appear in a number of sedimentary successions formed from the Late Permian to the Late Triassic in various depositional settings and under various diagenetic conditions, whereas only a negligible amount of dolomite was detected in the post-Triassic formations. Seven dolomite-bearing units representing ramp, small and large carbonate platforms, and intraplatform basin settings are presented in this synopsis. In most cases, multi-stage and polygenetic dolomitization was inferred. The main mass of the dolostones was formed via near-surface diagenetic processes, which were commonly preceded by the formation of synsedimentary dolomite. Accordingly, surficial conditions that prevailed during sediment deposition controlled the dolomite-forming processes and thus the lateral extension and the time span of dolomitization. The area of episodic subaerial exposure was a critical controlling factor of the lateral extension of the near-surface dolomite genesis, whereas its temporal extension was mostly governed by climate. Burial diagenesis usually resulted in only moderate dolomitization, either in connection with compactional fluid flow or via thermal convection. The Triassic fault zones provided conduits for fluid flow that led to both replacive dolomitization and dolomite cement precipitation. In the Late Triassic extensional basins, synsedimentary fault-controlled dolomitization of basinal deposits was reconstructed.

Keywords Diagenesis · Fault-related dolomite · Organogenic dolomite · Reflux · Stable isotopes · Thermal convection · Triassic · Tethys margin

Introduction

Dolostone and dolomitic limestone of Late Permian–Late Triassic age appear in a number of sedimentary successions in the Transdanubian Range (TR) of NW Hungary. They form large masses with a total thickness of 2.5–3 km, whereas only a negligible amount of dolomite was detected in the post-Triassic carbonate formations. A wide variety of dolostones and dolomite-bearing formations evolved in this domain, reflecting various depositional settings and diagenetic histories. In several cases, coeval completely dolomitized, partially dolomitized and non-dolomitized carbonates of similar depositional facies occur with preserved transitional intervals. Due to these characteristics, the TR can be considered as a natural laboratory providing a unique opportunity to study multi-phase dolomite genesis. The aim of this paper is to identify the main controlling factors of dolomite-forming processes by comparing a number of case studies of polygenetic dolostones formed on the Tethys margin during a given geologic time period.

✉ János Haas
haas@caesar.elte.hu

[1] MTA-ELTE Geological, Geophysical and Space Science Research Group, Pázmány P. sétány 1/c, Budapest 1117, Hungary

[2] Geological and Geophysical Institute of Hungary, Stefánia út 14, Budapest 1143, Hungary

[3] Noble Research Center, Boone Pickens School of Geology, Oklahoma State University, Stillwater, OK 74078, USA

[4] Research Centre for Astronomy and Earth Sciences, Institute for Geological and Geochemical Research, Hungarian Academy of Sciences, Budaörsi út 45, Budapest 1112, Hungary

[5] Present Address: ConocoPhillips Company, 600 N Dairy Ashford, Houston, TX 77079, USA

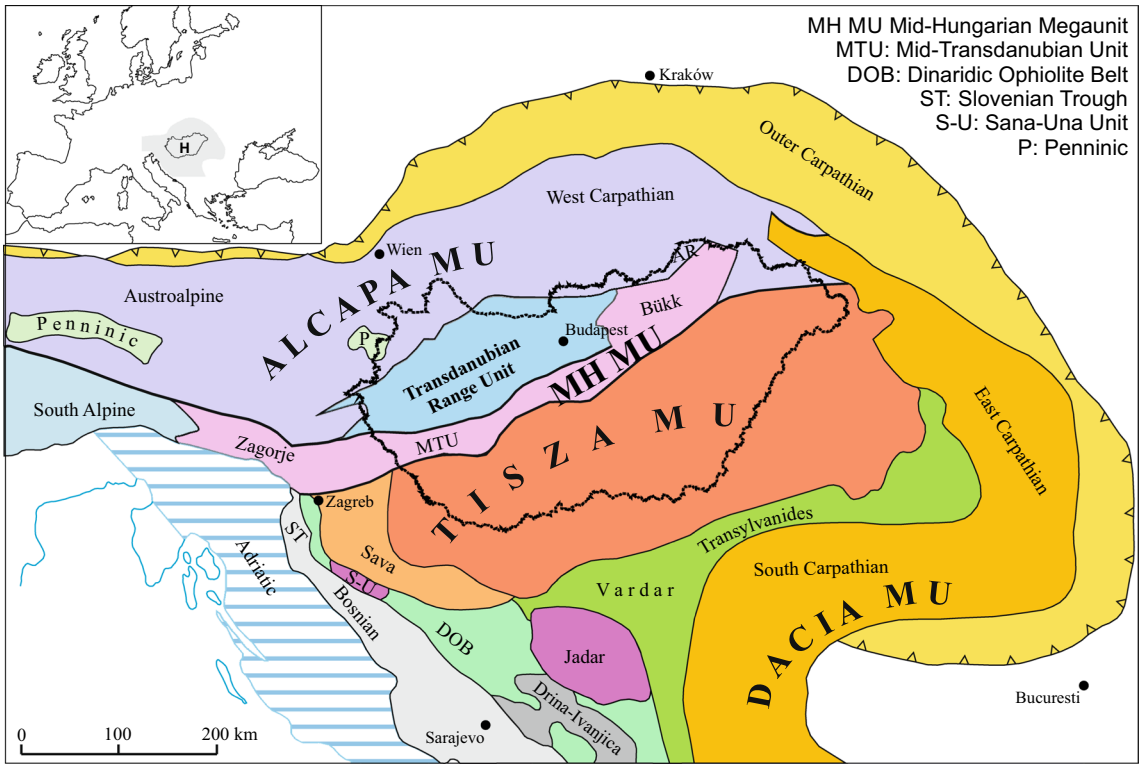

Fig. 1 Structural setting of the Transdanubian Range Unit in the Alpine–Carpathian–Dinaridic region (Haas et al. 2010)

Interpretation of dolomite-forming processes can help to reveal the relationship of dolomite genesis with palaeoenvironmental, depositional, diagenetic, and tectonic processes, and with certain stages of basin evolution. Inferences of our studies on various Triassic dolostones and dolomite-bearing units in the TR can be applied to evaluate the dolomitization history of similar successions formed in a vast region along the margin of the Tethys Ocean, and may also be considered for the interpretation of dolomite genesis under similar conditions in other regions and other periods of the Earth's history. Interpretation of dolomite-forming processes can provide a basis for the analysis of their relationships with depositional, diagenetic, and tectonic processes and stages of basin evolution, with significant implications for hydrocarbon exploration and hydrogeologic research.

Geologic setting

The Transdanubian Range (TR) is a NE–SW-trending chain of moderately elevated mountains and hills, extending for a length of about 200 km (Figs. 1, 2). The Transdanubian Range Unit is an Upper East Alpine (Austroalpine)-type nappe, which was not affected by Alpine metamorphism (Fodor et al. 2003; Tari and Horváth 2010). In the early period of the Alpine plate-tectonic cycle the TR was located between the South Alpine and Upper East Alpine realm, as a segment of the Adriatic margin of the Neotethys Ocean (Fig. 3; Haas et al. 1995; Mandl 2000; Gawlick 2000).

After a long continental rifting stage from the Late Permian to the early period of the Middle Triassic, the opening of the Neotethys Ocean commenced during the middle part of the Middle Triassic in the Alpine–Carpathian–Dinaric domain (Csontos and Vörös 2004). In connection with the opening, crustal extension led to development of a segmented topography also along the continental margins of the young narrow oceanic basin; grabens and submarine highs came into being (Budai and Vörös 1992). The opening of the ocean continued during the Late Triassic to Early Jurassic. On large parts of the passive margin thick platform, carbonate successions were formed, whereas much thinner pelagic sequences accumulated in the basins (Haas et al. 1995). In the course of the ocean opening, attenuation of the crust continued. This resulted in the acceleration of the subsidence and downfaulting of blocks in the near-oceanic external belt of the continental margin, which is manifested in step-by-step drowning of the carbonate platforms from the latest Triassic to the Early Jurassic.

The main stages of the evolution of the depositional area of the TR in the studied time range are the following (Budai and Vörös 1992; Budai et al. 1993; Haas and Budai

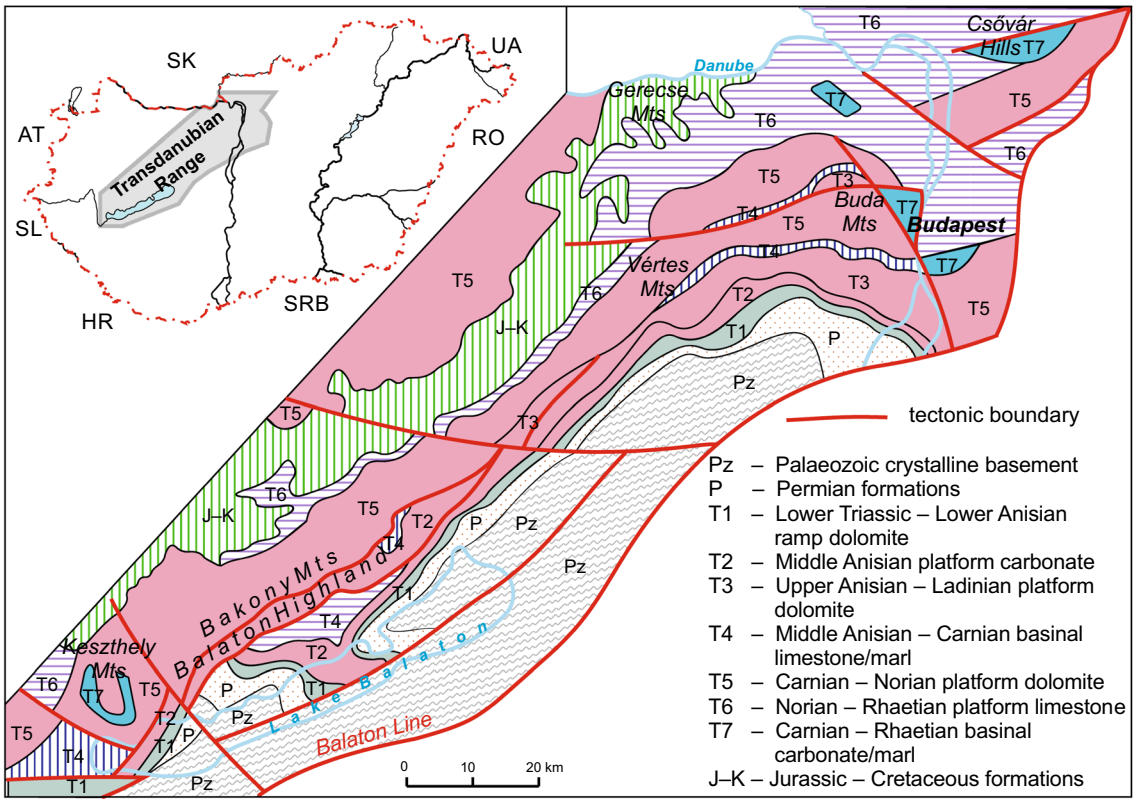

Fig. 2 Pre-Cenozoic geologic map of the Transdanubian Range (TR; modified after Haas et al. 2010). The *grey shading* on the *inset map* shows the displayed segment of the unit within Hungary

1995, 1999; Budai and Haas 1997; Haas 2012; Haas et al. 2012; Figs. 4, 5):

- Late Permian transgression, leading to the establishment of alluvial plain (Balatonfelvidék Sandstone), coastal sabkha (Tabajd Formation), and shallow marine lagoonal environments (Dinnyés Dolomite) under semi-arid to arid climatic conditions.
- Marine inundation of the entire TR area at the Permian/Triassic boundary, followed by mixed siliciclastic–carbonate shallow ramp sedimentation during the Early Triassic (Köveskál, Arács and Alcsútdoboz Formations), mostly during a semi-arid climate with a significant humid pulse in the early Olenekian (Hidegkút and Csopak Formations).
- Cessation of siliciclastic input led to carbonate deposition on the ramp during the Early Anisian (Aszófő and Megyehegy Dolomite, Iszkahegy Limestone), still under arid to semi-arid climatic conditions.
- As a consequence of the Middle Anisian extensional tectonic activity the former carbonate ramps were dissected along normal faults. Asymmetric hemipelagic basins came into existence above the downfaulted blocks (Felsőörs Limestone), whereas isolated carbonate platforms evolved on the relatively elevated ones (Tagyon Formation). Larger platforms developed during the latest Anisian to earliest Carnian interval (Budaörs Dolomite), and volcanic tuff interbeds formed along with hemipelagic carbonates in the basins (Buchenstein and Füred Formations). The semi-arid climate persisted during this evolutionary stage.
- Humid climate in the late Early Carnian (Carnian Pluvial Event) led to the onset of filling up of the intraplatform basins by fine siliciclastic sediments (Veszprém and Csákberény Formations). The basin infill was completed during the early Late Carnian in the south-western part of TR (Sándorhegy Formation), whereas new basins developed in the north-eastern part of the area (Mátyáshegy and Csővár Limestone Formations).
- Levelled topography gave rise to the development of an extremely extended carbonate platform system in the latest Carnian. Semi-arid climate prevailed during the first stage of the platform evolution (Fődolomit Formation; equivalent of Hauptdolomit and Dolomia Principale, respectively), which gradually changed to semi-humid conditions in the middle part of the Norian (Dachstein Limestone).

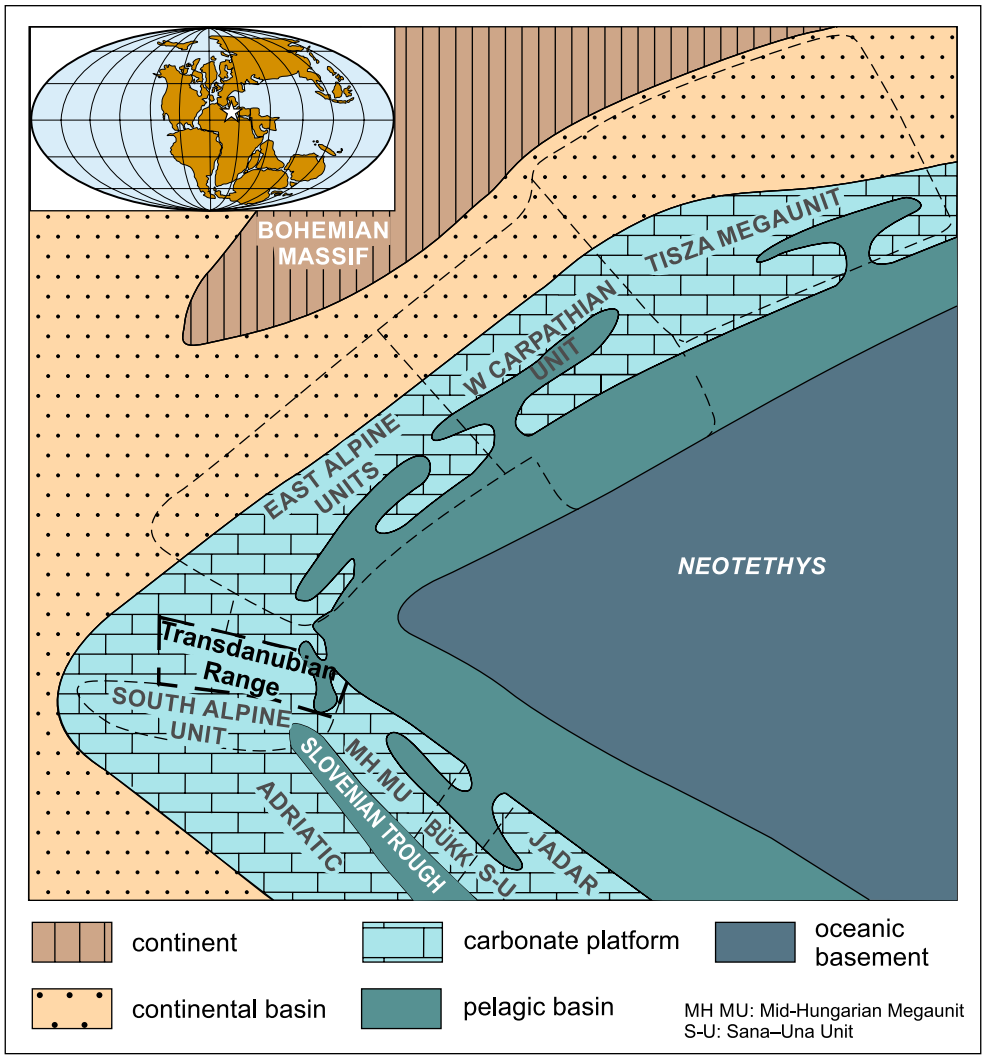

Fig. 3 Palaeogeographic setting of the Transdanubian Range Unit (modified after Haas et al. 1990)

- A large extensional basin formed in the south-western part of the TR in the Late Norian to Rhaetian, in connection with the opening of the Penninic Ocean basin (Alpine Tethys). In the Rhaetian, as a result of the increasing humidity, carbonate sedimentation (Rezi Dolomite) was replaced by deposition of fine siliciclastic sediments (Kössen Formation) in this basin.

The extensional regime was maintained and differential subsidence continued during the Jurassic into the Early Cretaceous. Above an attenuated continental crust, pelagic carbonate sediments formed on the articulated bottom, and the Permian–Triassic formations reached the deep burial zone (2–5 km). A crucial compressional deformation event occurred in the mid-Cretaceous that resulted in the formation of the large synclinal structure of the TR (Haas 2012 and references therein). This was followed by uplift and intense erosion during the Turonian–Coniacian interval that resulted in the denudation of the entire Jurassic–Lower Cretaceous succession and even a large part of the Triassic sequence in the limbs of the syncline (Haas 2012 and references therein). Accordingly the Triassic carbonates were first raised to a near-surface position at this time. Similar tectonically controlled uplift, denudation and fracturing occurred in several stages during the Cenozoic. The fault-related fluid circulation and telogenetic processes (calcitization, precipitation of fracture-filling cements and locally hydrothermal minerals, powderization) significantly altered or completely destroyed the original fabric of the dolostones over large parts of the TR (e.g. Esteban et al. 2009; Győri et al. 2011; Poros et al. 2012, 2013).

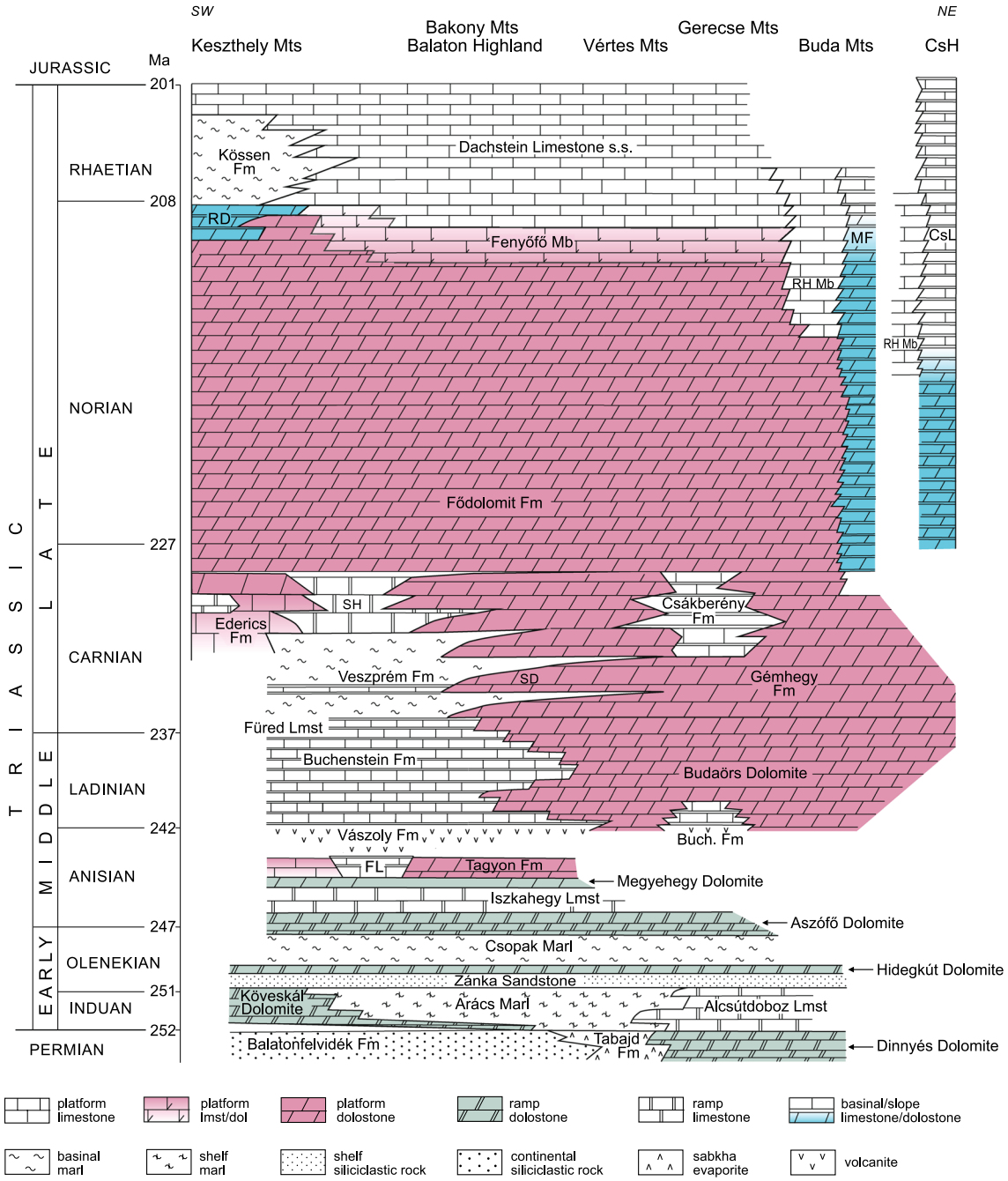

Fig. 4 Stratigraphic setting of the dolostones and dolomite-bearing formations in the TR (modified after Haas and Budai 1995, 1999). Abbreviations: *CsH* Csővár Hills, *FL* Felsőörs Limestone Formation, *SD* Sédvölgy Dolomite Member, *SH* Sándorhegy Formation, *RD* Rezi Dolomite Formation, *MF* Mátyáshegy Formation, *CsL* Csővár Limestone Formation, *RH Mb* Remetehegy Member

Materials and methods

This paper is mostly based on the investigation of samples collected during the past 5 years within the framework of a project dedicated to the study of dolostones in the TR. Twenty-one natural outcrops and quarries and 13 cored wells were sampled. A total of 141 samples were taken for petrographic, mineralogical and geochemical studies. In addition to the new samples, petrographic analyses were carried out on about 1600 archive thin sections prepared previously during geological mapping projects and the National Key Section Project. The samples and thin

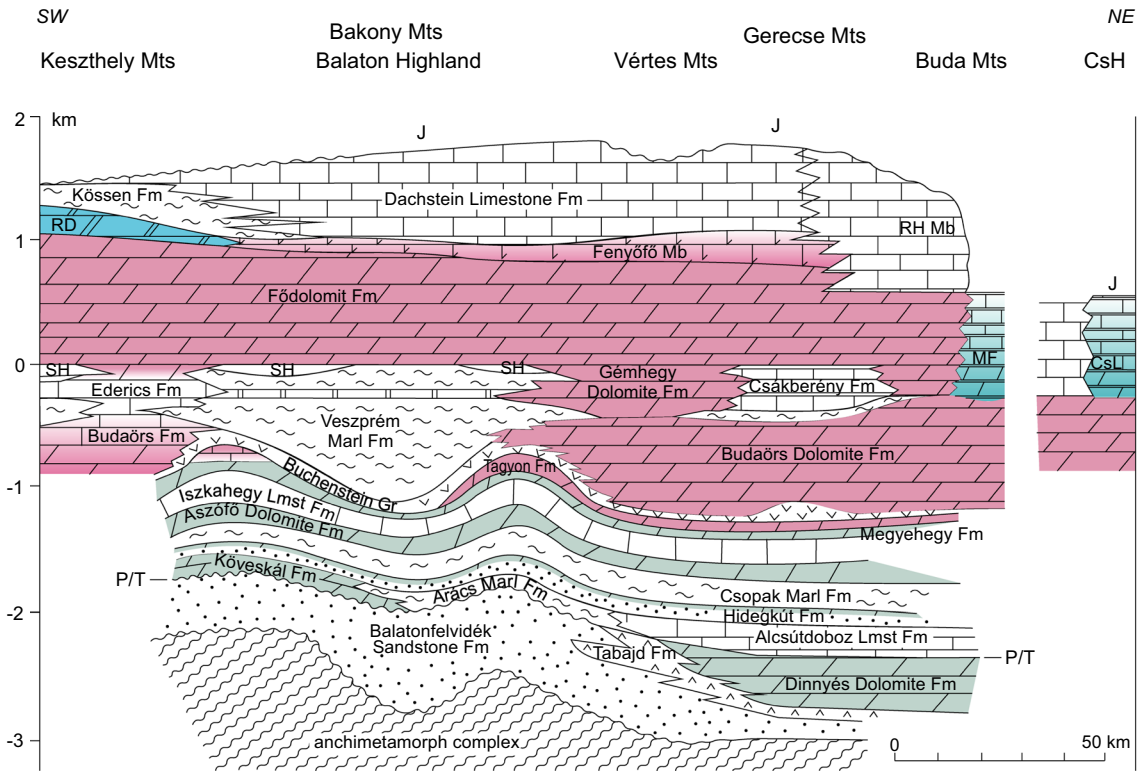

Fig. 5 Conceptual cross section of the TR, showing the thickness and the relationship of the Triassic formations (after Haas and Budai 1995). The base of Fődolomit formation is chosen for the reference (0) level, because peritidal beds of this formation of overall extension in the TR was deposited onto levelled topography. The legend is identical with that of Fig. 4. Abbreviations: *CsH* Csővár Hills, *J* preserved Jurassic formations, *P/T* Permian/Triassic boundary, *RD* Rezi Dolomite Formation, *SH* Sándorhegy Formation, *RH Mb* Remetehegy Member, *MF* Mátyáshegy Formation, *CsL* Csővár Limestone Formation

sections are stored in the repository of the Geological and Geophysical Institute of Hungary and in the collection of the MTA-ELTE Geological, Geophysical and Space Science Research Group.

The methods used in the studies of the project were described in the following papers: Haas et al. (2014a, b, c, 2015) and Hips et al. (2015, 2016). Investigation of fluid inclusions was possible only in three cases (studies of Middle Triassic dolomitized platform carbonates; Carnian dolomitized reef limestone; Carnian-Norian dolomitized slope and basinal carbonates) due to lack of suitable inclusions. The majority of the stable isotope data presented here had been published in the previously listed research papers; however, the data of the Lower Triassic and the Anisian carbonates are first published here. The samples were taken by a dental drill, but in most cases the selective sampling was not successful due to the small size of the components, therefore the data are marked as bulk on the diagram. All the samples of the project were measured in the Institute for Geological and Geochemical Research of the Hungarian Academy of Sciences, using the same instrument. The analyses were carried out using the continuous flow technique (Spötl and Vennemann 2003), and the calcite and dolomite reaction conditions and fractionation factors described by Rosenbaum and Sheppard (1986). The $^{13}C/^{12}C$ and $^{18}O/^{16}O$ ratios were determined in CO_2 gases liberated by phosphoric acid using a Finnigan delta plus XP mass spectrometer (Thermo Fisher Scientific, Bath, UK). Standardization was conducted using laboratory calcite standards calibrated against the NBS 18 and NBS 19 standards. During the measurement of the dolomite samples a laboratory dolomite standard (DST; calibrated to NBS-19 in analyses at 25 °C) was used. All samples were measured at least in duplicate, and the mean values are in the traditional δ notation in parts per thousand (‰) relative to Vienna Pee Dee Belemnite (VPDB). Reproducibility is better than ±0.1 ‰ for $\delta^{13}C$ and ±0.15 ‰ for $\delta^{18}O$.

Petrographic and geochemical characteristics of the dolomite-bearing formations and interpretation of the dolomite-forming processes

Characteristics of the investigated Triassic dolomite-bearing formations are summarized in Table 1, and the stable

Table 1 Lithology/lithofacies types of the studied rock bodies, paragenetic sequence of the dolomite phases and interpretation of the dolomite-forming processes

Chronostratigraphic units, depositional facies	Lithostratigraphic units	Lithofacies types or lithology	Dolomite phases in paragenetic sequences	Processes	Diagenetic realm
7. Carnian-Norian dolomitized slope and basinal carbonates	Mátyáshegy Formation, Csővár Formation	dolomitic limestone laminated dolostone massive dolostone	1. finely to coarsely crystalline replacive dolomite 2. coarsely crystalline dolomite cement	fault-controlled, buoyancy-driven convection fault-controlled, buoyancy-driven convection	intermediate burial intermediate burial
6. Carnian-Norian dolomitized and partially dolomitized platform carbonates	Gémhegy Dolomite, Fődolomit Formation, Fenyőfő Member	Lf A calcrete/dolocrete Lf B stromatolite Lf C massive dolostone and dolomitic limestone (wackestone/packstone/grainstone)	1. finely crystalline dolomite aggregates 2. very finely to medium crystalline replacive dolomite 3. finely to coarsely crystalline dolomite cement	organogenic precipitation reflux fault-related	synsedimentary near-surface intermediate burial
5. Carnian partially and selectively dolomitized reef limestone	Ederics Limestone	non-dolomitized to slightly dolomitized reef limestone selectively dolomitized reef limestone dolostone with calcareous remnants dolostone	1. finely crystalline dolomite aggregates 2. finely to coarsely crystalline replacive dolomite 3. medium to coarsely crystalline dolomite/calcite cement	organogenic precipitation compaction-related fluid flow fault-related	synsedimentary intermediate burial intermediate burial
4. Middle Triassic (uppermost Anisian-Ladinian) dolomitized platform carbonates	Budaörs Dolomite	thin-bedded/laminated dolostone massive dolostone	1. aphanocrystalline dolomite precipitate 2. finely crystalline replacive dolomite 3. medium crystalline replacive dolomite 4. dolomite overgrowth cement	organogenic precipitation tidal pumping in mesohalin setting pervasive, thermal convection pervasive, thermal convection	synsedimentary synsedimentary intermediate burial intermediate burial
3. Middle Anisian platform dolostone (**a**) and dolomitic limestone (**b**)	Tagyon Formation	Lf A calcrete/dolocrete Lf B stromatolite Lf C massive dolostone, dolomitic limestone, limestone (boundstone/grainstone)	1. finely crystalline dolomite aggregates 2. very finely to finely crystalline replacive and cement dolomite 3. finely to medium crystalline replacive dolomite 4. (**a**) finely to medium crystalline replacive dolomite 5. medium to coarsely crystalline cement; (**a**) dolomite, (**b**) calcite+dolomite	organogenic precipitation combination of pedogenic and reflux reflux pervasive, thermal convection fault-related	synsedimentary synsedimentary/near-surface near-surface intermediate burial intermediate burial
2. Lower Anisian ramp dolostone	Aszófő Dolomite	dolostone dolostone with evaporite nodules	1. very finely to finely crystalline replacive dolomite 2. medium to coarsely crystalline dolomite cement	reflux reflux	near-surface near-surface
1. Lower Triassic dolomitized shallow-marine mixed siliciclastic-carbonate rocks	Köveskál Dolomite, Arács Marl, Alcsútdoboz Limestone, Hidegkút Formation, Csopak Formation	calcareous/dolomitic siltstone and sandstone silty and sandy dolostone dolostone dolomitic limestone limestone	1. very finely to medium crystalline replacive dolomite 2. finely to coarsely crystalline replacive and cement ferroan dolomite-ankerite	reflux fault-controlled brine-mixing	near-surface intermediate burial

isotope values measured in dolomite samples of the studied formations are presented in Fig. 6.

Lower Triassic (Induan–Olenekian) dolomitized shallow marine mixed siliciclastic-carbonate rocks

The Lower Triassic succession of the TR is made up mainly of carbonates with variable amounts of siliciclastics (Haas et al. 1988). During the Induan, the sediments were deposited in tidal flat, lagoon and ooid shoal environments (Köveskál Dolomite, Arács Marl, and Alcsútdoboz Limestone Formations; Fig. 4). Following siliciclastic sedimentation during a humid episode, sea level drop and a decrease in terrigenous input (Haas et al. 2012) led to the formation of shallow lagoonal carbonates (Hidegkút Dolomite). During the late Olenekian, silty marl with partially dolomitized carbonate tempestite interlayers were deposited in a middle to outer ramp setting (Csopak Marl Formation; Fig. 4). A strikingly similar Lower Triassic succession (Werfen Formation) occurs in the Southern Alps; peritidal dolostones in the Induan (Andraz Horizon), and the upward shallowing Olenekian succession (Cencenighe and San Lucano Members) (Broglio Loriga et al. 1990).

Five lithofacies types have been differentiated in the studied cores, such as dolomitic siltstone and sandstone (Fig. 7a, b), silty and sandy dolostone, dolostone (Fig. 7c), dolomitic limestone (Fig. 7d) and limestone. The siliciclastic rocks are made up of quartz, quartzite, mica, glauconite grains and other clay minerals. Replacive dolomite and ankerite were found in the first two lithofacies types; either as poikilotopic crystals enclosing quartz grains (Fig. 7a) or as fine-to medium crystals among the quartz grains (Fig. 7b). The crystals exhibit zonation as revealed by SEM-BE. The fabric-preserving and fabric-destructive dolomite textures are characterized by nonplanar-anhedral crystals of various sizes ranging from very fine to medium (Fig. 7c). The replacive dolomite is either non-ferroan or ferroan, and a ferroan dolomite overgrowth rim was observed on some crystals in fractures or vugs. In the dolomitic limestone lithofacies coarse subhedral ferroan dolomite crystals replaced the bioclasts and ooids, whereas the intergranular pore space is filled by calcite and ferroan calcite (Fig. 7d). The replacive dolomite crystals exhibit undulose extinction in all lithofacies. Microfacies of the limestone is nodular mudstone, bioclastic wackestone and grainstone. All rock types are cut across by fractures cemented with coarse dolomite cement.

The presence of sulphates, namely gypsum and anhydrite (Fig. 7b), characterizes the dolomitic siltstone and sandstone. These minerals occur as poikilotopic crystals

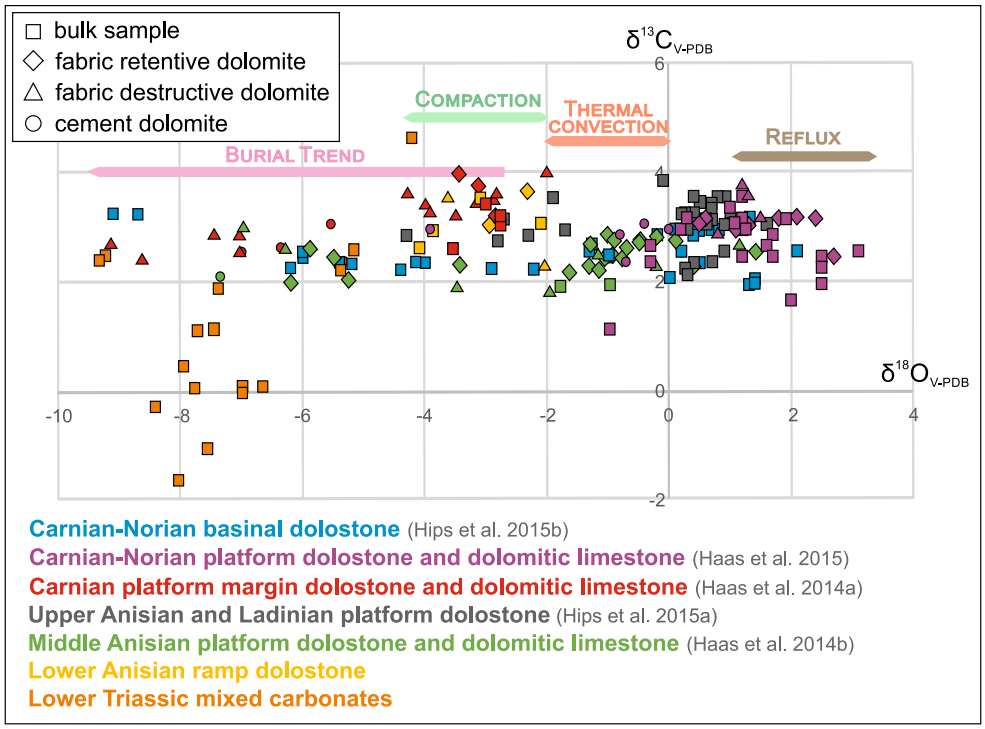

Fig. 6 Stable isotope values measured in dolomite samples from the TR. The *arrows* illustrate ranges of values, which are interpreted as being typical for the indicated dolomite-forming processes in the Triassic succession of TR. The plot is primarily based on previously published data (for references see the legend included in the figure)

in patches, as fibrous crystals filling fractures and anastomosing vugs, and also as nodules. Barite and sulphides (pyrite, sulphosalts, subordinately galena and chalcopyrite) post-date all the previous minerals and occur in fractures or form patches in all the various lithofacies types.

Pressure dissolution resulted in the formation of stylolites. Replacive dolomite was locally observed along stylolites. Ferroan calcite replaces some of the dolomite in the dolomitic limestone, and it also appears as a fracture-fill both pre- and post-dating stylolitization.

Stable isotope geochemistry

The stable oxygen and carbon isotope pattern of the Lower Triassic rocks are characterized by negative $\delta^{18}O$ and both negative and positive $\delta^{13}C$ values (Fig. 6). The $\delta^{18}O$ values range from −9.3 to −4.2 ‰, whereas the $\delta^{13}C$ values range from −1.6 to 4.7 ‰.

Interpretation

The petrographic features suggest multistage dolomitization. The first stage of the dolomitization took place in the shallow burial realm, as proposed earlier by Haas et al. (1988). Occurrence of gypsum and anhydrite in the Induan beds indicates arid conditions. Accordingly, reflux circulation of fluids within the sedimentary succession is assumed. The observed replacive non-ferroan, nonplanar-anhedral dolomite likely belongs to this stage. A more humid climate in the Olenekian most probably terminated the reflux of the fluids. The lack of the non-ferroan replacive dolomite phase in the Olenekian rocks is in accordance with this assumption.

The ferroan dolomite, ankerite, barite and sulphide paragenesis represents a subsequent event in the diagenetic history of the Lower Triassic rocks. This mineral association suggests an influx of metal-transporting fluids, which ascended along faults from the underlying Permian evaporite and red sandstone beds. The fluids reacted with the wall rocks and became acidic and reducing (cf. Dill 2010). This resulted in (1) dissolution and transport of Fe and other cations (such as Sb, As, Cu, Zn, Hg), most probably from the Permian red sandstone, (2) dissolution of vugs in the Lower Triassic limestone/dolostone, (3) replacement of the remaining calcite phases by ferroan dolomite–ankerite, and (4) precipitation of sulphides and barite in the last stage.

Stable C-isotope values of most of the Lower Triassic samples are more negative than all the other investigated dolomites, which is in accordance with the documented negative shifts on C-isotope curves representing the

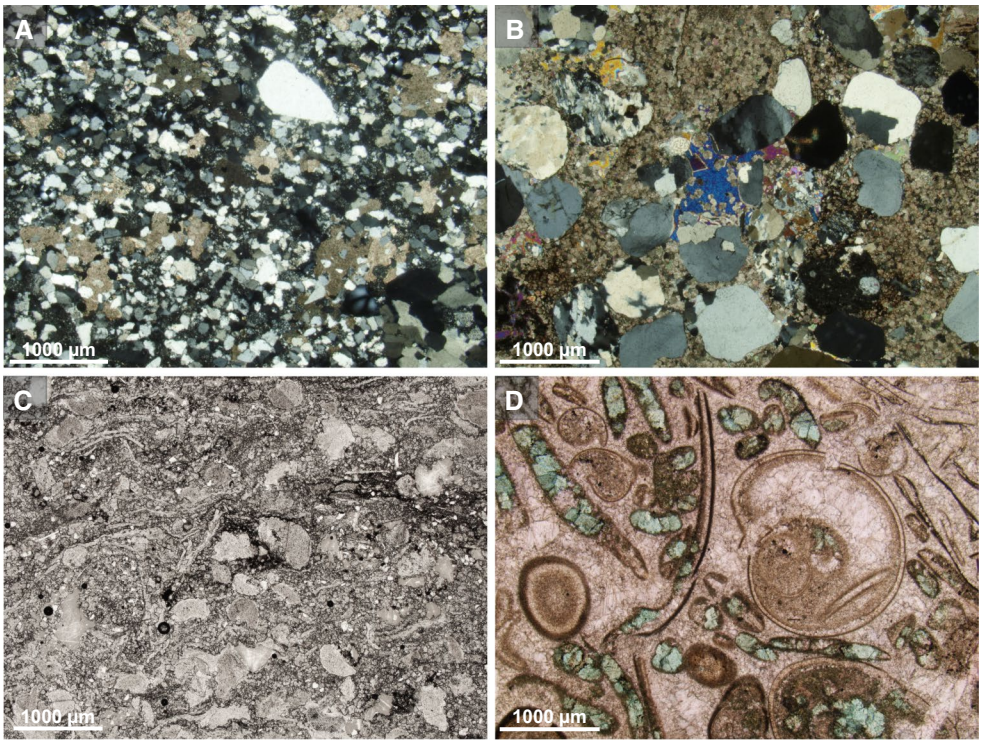

Fig. 7 **a** Nonplanar-anhedral dolomite among quartz grains in dolomitic sandstone, crossed polars, well Kk-9, 377.7 m (Köveskál Dolomite Formation). **b** Nonplanar-anhedral dolomite-ankerite among quartz and quartzite grains in dolomitic sandstone, crossed polars, well Bsz-3, 887.5 m (Hidegkút Formation). **c** Skeletal fragments of echinoderms and molluscs in fabric retentive dolomite, stained thin section, well Kk-9, 356.2 m (Köveskál Dolomite Formation). **d** Ferroan dolomite replaces bioclasts in dolomitic limestone, stained thin section, well Gát-1, 277.6 m (Arács Marl Formation)

aftermath of the Permian–Triassic boundary event (cf. Corsetti et al. 2005). The reasons put forward are: (1) release of methane from gas hydrates, (2) input of CO_2 of volcanic origin, and (3) release of CO_2 from the degrading biomass caused by the mass extinction (Corsetti et al. 2005). The negative oxygen isotope data could be explained by the elevated temperature of the metal-bearing, dolomitizing fluid, but a proposed increase of 8 °C in tropical sea surface temperatures has to be taken into consideration, as well (Joachimski et al. 2012).

Lower Anisian ramp dolostone

In the early Anisian, carbonate deposition became prevailing on the shallow ramp as a result of significant reduction in the fine terrigenous siliciclastic input; 50- to 250-m-thick, laminated to thin-bedded dolomite was formed (Aszófő Dolomite Formation; Fig. 4). In many cases, the sedimentary fabric of the precursor rock was completely destroyed by dolomitization but successions with moderately to well-preserved sedimentary fabric also occur. In the latter cases, cyclic alternation from shallow subtidal to evaporite-bearing supratidal facies was observed (Haas et al. 1988). There is a tens of metres thick transition zone between the entirely dolomitized formation and the overlying limestone. The transitional section is characterized by alternation of dolomitized and non-dolomitized intervals.

Similar to the TR, Lower Anisian inner ramp dolomites are also widespread in the Dolomites (Lower Serla Dolomite), in Lombardy (Carniola di Bovegno) (De Zanche et al. 1993; Gianolla et al. 1998) and in the Northern Calcareous Alps (Reichenhalle Formation) (Spötl and Burns 1991).

Based on microfacies investigations, completely dolomitized oolitic grainstone and peloidal wackestone characterize the lower part, whereas peloidal wackestone or mudstone is common in their upper part of the cycles. In the latter part, mm-sized anhydrite and gypsum nodules, dolomite–calcite pseudomorphs after gypsum crystals (Fig. 8a, b), and pores after dissolution of evaporites were observed. The matrix is usually replaced by very finely crystalline dolomite. Micritized bioclasts and ooids are common, although dolomite cement-filled moulds of molluscs also occur. In certain laminated evaporite-bearing deposits, desiccation cracks and rip-up clasts are common.

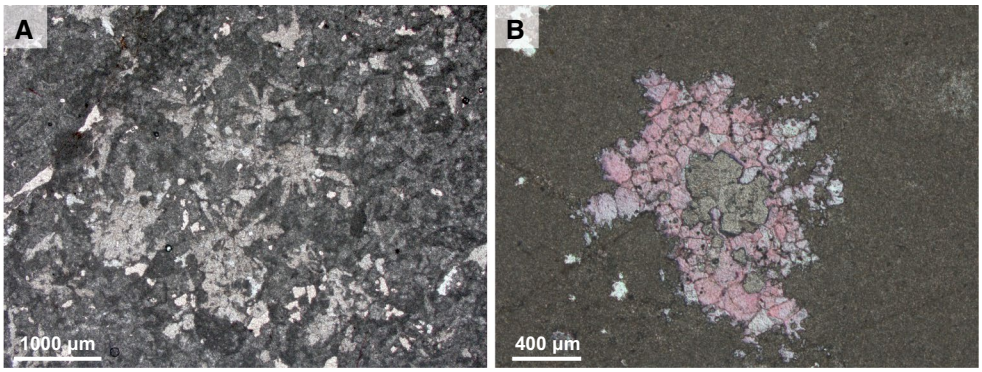

Fig. 8 Photomicrographs showing characteristic features of evaporitic wackestone–mudstone facies that commonly occur in the upper part of the depositional cycles (Aszófő Formation). **a** Medium crystalline dolomite with calcite-filled moulds after dissolution of gypsum crystal aggregates. Stained thin section. Road cut exposure at Aszófő, Balaton Highland. **b** Coarse crystalline dolomite with cement-filled dissolution pores after evaporates. The pore is filled by medium-to-coarse crystalline mosaic calcite and dolomite. In some cases, the dolomite occurs in the form of inclusion within calcite crystals. Stained thin section. Well Bsz-3. 658 m

Stable isotope geochemistry

The $\delta^{13}C$ and $\delta^{18}O$ values of the samples taken from completely dolomitized peloidal and mudstone deposits are within a rather narrow range; $\delta^{13}C$ from 2.3 to 3.1 ‰ and $\delta^{18}O$ from −4.1 to −2.1 ‰ (Fig. 6).

Interpretation

Decreasing terrigenous input at the beginning of the Anisian reflects increasing aridity, which was accompanied by rising sea level (Haas et al. 2012). Oolite shoals were established in the high-energy parts of the carbonate ramp and carbonate mud deposited in the protected low-energy back-shoal zone. The subsequent sea level fall led to increasing restriction of the inner platform and, accordingly, to increasing salinity. This is reflected in the low diversity fossil assemblage (Haas et al. 1988). In the hypersaline water, gypsum crystals were precipitated, which were transformed into nodules during diagenesis. On the prograding mudflat, sabkha with ephemeral pools formed. Reflux of the evaporated sea water caused complete dolomitization of the previously deposited evaporite-bearing carbonate sediment. The $\delta^{18}O$ values are somewhat depleted in ^{18}O, which seems to be in contradiction to the reflux dolomitization. However, the extremely hot climate, which prevailed from the Permian–Triassic boundary until the early Anisian (Joachimski et al. 2012; Sun et al. 2012), may have caused a negative shift of the $\delta^{18}O$ values. This interpretation is also supported by similarly depleted values reported from coeval evaporitic dolostone (Reichenhall Beds) in the Northern Calcareous Alps (Spötl and Burns 1991). The cycle of shallow marine carbonate accumulation during rising sea level, and reflux dolomitization during subaerial exposure periods, was repeated several times due to changes in sea level. The long-term trend of rising sea level later led to cessation of recurring subaerial exposure episodes, which in turn terminated the dolomitization processes.

Middle Anisian platform dolostone and dolomitic limestone

Disintegration of the carbonate ramp led to formation of small platforms and deeper basins in the Middle Anisian. On the platforms, 50- to 100-m-thick cyclic platform carbonate sequences were formed (Tagyon Formation; Fig. 4). The metre-scale cycles consist of subtidal beds with fragments of shallow marine fossils, intertidal stromatolite beds and calcrete/dolocrete caps. Most of the platform carbonates were subjected to complete dolomitization. However, a small platform in the area of the Balaton Highland consists mostly of limestone with both partially and entirely dolomitized intervals (Haas et al. 2014b).

The corresponding isolated platforms of the Southern Alps are either partially dolomitized (e.g. the Upper Serla Formation and the Contrin Formation) in the Dolomites, or non-dolomitized (e.g. Dosso dei Morti Limestone in Lombardy, Gaetani et al. 1981; De Zanche et al. 1993; Gianolla et al. 1998).

In the partially dolomitized rock bodies, various fabric-selective dolomite types were observed. In the cap horizons, pedogenic nodules, glaebules, and coated grains are mostly composed of very finely to finely crystalline dolomite, although the intragranular micropores are generally filled by very finely crystalline calcite, and less frequently by dolomite of similar crystal size (Fig. 9a, b). The dolomitic stromatolite beds exhibit clotted micrite microfabric. In the subtidal beds, scattered, irregular aggregates of very finely crystalline dolomite, and/or 15- to 200-µm-sized

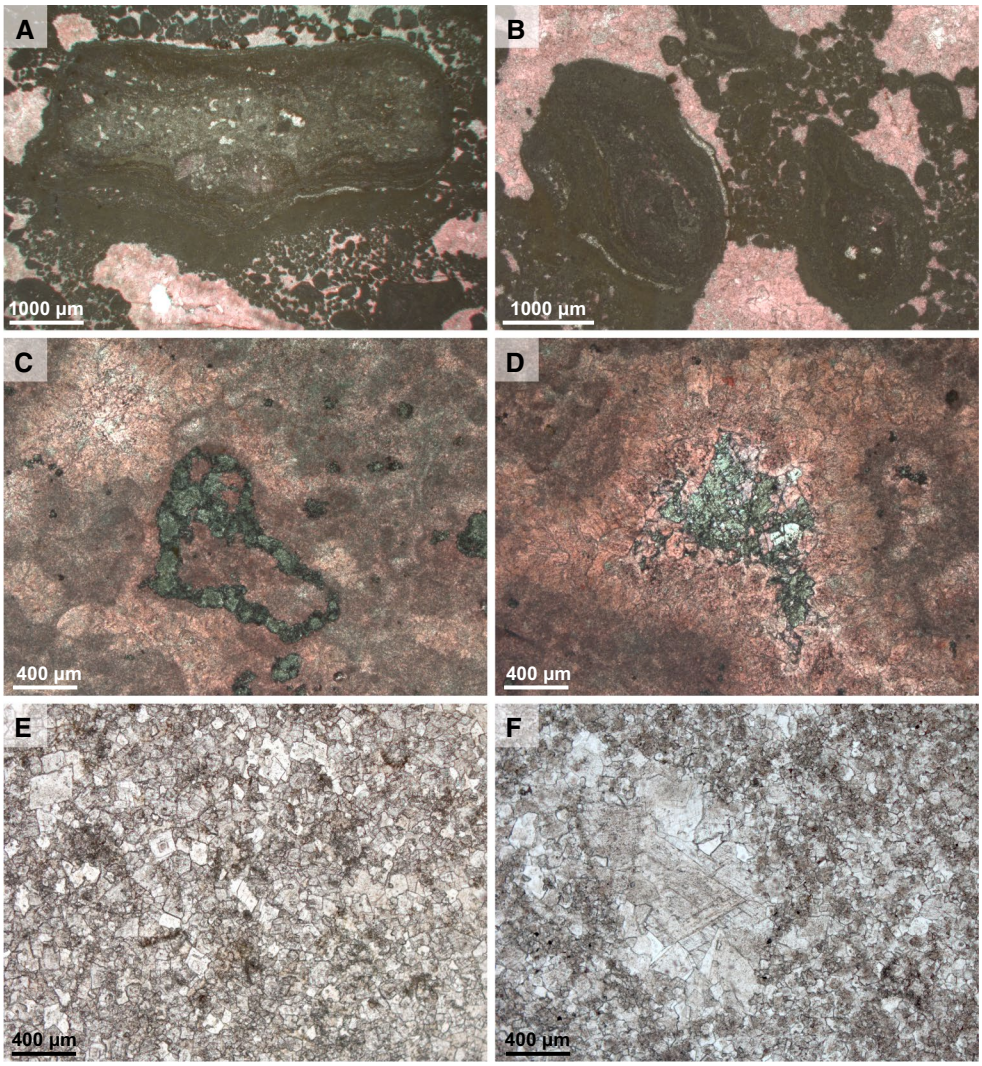

Fig. 9 Photomicrographs showing characteristic fabrics of the partially dolomitized rock bodies (Tagyon Formation). **a** and **b** Pedogenic glaebules and mm-sized coated grains composed of very finely to finely crystalline dolomite. The intragranular micropores are filled by finely crystalline calcite. The irregular pores among the grains are usually lined by inclusion-rich bladed calcite whereas medium crystalline mosaic calcite cement fills the inner part of the pores. Stained thin section; well Drt-1, 125.4 m. **c** Micrite nodule with clusters of euhedral to anhedral dolomite. Stained thin section; well Drt-1, 112.6 m. **d** Coarsely crystalline calcite and coarsely crystalline dolomite vug-filling cement phases. Stained thin section; well Drt-1, 112.6 m. **e** Fine-to-medium crystalline planar-euhedral-subhedral dolomite; stained thin section; well Drt-1, 75.8 m. **f** Coarsely crystalline planar-subhedral dolomite in medium crystalline nonplanar-anhedral and planar-subhedral dolomite; well Drt-1, 84.9 m

euhedral, subhedral and anhedral dolomite crystals or crystal clusters occur in the micritic fabric elements (small peloids, micritic nodules, cortex of oncoids, and micritic envelope of various grains) testifying micrite-selective dolomitization. The small pores among the micrite nodules are occluded by finely crystalline calcite cement. The mm- to cm-sized vuggy pores are lined by calcite cement. Coarsely crystalline mosaic calcite and/or coarsely crystalline dolomite occur in the central part of the vugs (Fig. 9d).

In several horizons, mostly in the uppermost 20 m of the formation, entirely dolomitized rocks occur. In these intervals, fabric-destructive dolomite prevails, although ghosts of some grains (e.g. peloids, bioclasts, and oncoids) are locally recognizable. This dolomite is typically fine-to-medium crystalline, exhibiting planar-subhedral and nonplanar-anhedral texture (Fig. 9c) with coarsely crystalline dolomite cement in vugs (Fig. 9d). Saddle dolomite occurs locally as the last cement phase in these vugs.

In the completely dolomitized part of the formation (in the north-eastern part of the Balaton Highland; Figs. 4, 5), the pedogenic and microbial fabric in the upper part of the cycles is well preserved (Fig. 10a–c). In the subtidal beds, dolomitization usually preserved the sedimentary fabric and the crystal morphology of the precursor early

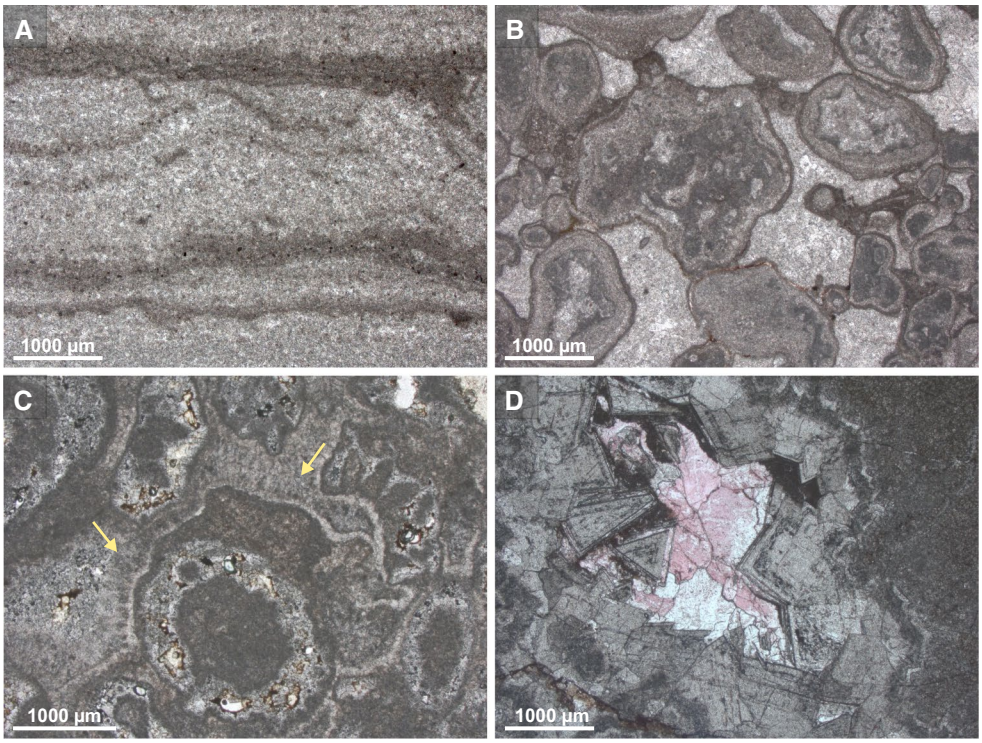

Fig. 10 Photomicrographs showing characteristic fabrics of the completely dolomitized rock bodies (Tagyon Formation). **a** Stromatolite with aphanocrystalline prostrate threads and faint clotted micrite, surrounded by very fine-to-fine crystals. Szentkirályszabadja Quarry. **b** Pedogenic coated grains. Both the grains and the intergranular cement were subjected to micritization, microsparitization and replacive dolomitization. Szentkirályszabadja Quarry. **c** Bioclastic grainstone. Clotted micrite envelope preserved the outlines of the dasycladalean algae fragments and filled their internal hollow. The biomoulds are filled by finely crystalline dolomite. Dolomitized fibrous cement (*arrows*) occurs between the micrite-coated skeletal fragments (which were later dissolved). Szentkirályszabadja Quarry. **d** Vugs with coarsely crystalline zoned dolomite cement. In the *central* part, late-stage calcite cement precipitated, post-dating the dissolution of dolomite crystals. Stained thin sections

diagenetic cements. However, in many cases, only ghosts of the grains are visible. In some beds, biomoulds after dasycladalean algae are abundant. Fibrous dolomitized cement occurs locally among the remnants of dasycladalean algae (Fig. 10c). The smaller vugs are filled with fine-to-medium crystalline dolomite, whereas medium-to-coarse dolomite cement occurs in the larger (mm-sized) vugs (Fig. 10d).

Stable isotope geochemistry

There is a remarkable difference between the $\delta^{18}O$ values of the dolomites from the pervasively dolomitized and the partially dolomitized successions, whereas the $\delta^{13}C$ values are similar (1.1–2.9 ‰ for the completely dolomitized and 1.4–3.0 ‰ for the partially dolomitized sequences; Fig. 6; for further details see Haas et al. 2014b).

The $\delta^{18}O$ values of calcite cements sampled from the partially dolomitized succession yielded −2.9 ‰ for fibrous calcite, and −4.4 ‰ for fracture-filling bladed calcite. Bulk samples taken from the slightly dolomitized limestone with micrite matrix and pore-filling calcite cement yielded more negative $\delta^{18}O$ values (−5.7 and −5.4 ‰). These values are within the range measured on bulk samples of fabric retentive and fabric-destructive dolomite (−6.2 to −3.4 ‰). The most negative $\delta^{18}O$ values were measured in coarsely crystalline calcite cement (−7.3 ‰) and in medium-to-coarse crystalline dolomite cement (−7.4 ‰).

The $\delta^{18}O$ values measured on bulk samples of fabric retentive, moderately to poorly fabric retentive and fabric-destructive samples of the pervasively dolomitized succession range between −2.0 and +1.4 ‰. The separately sampled dolomitized cements (replaced fibrous and bladed calcite cement) are characterized by values of −2.2 to 0.1 ‰. The most negative $\delta^{18}O$ value (−3.9 ‰) was measured on medium-to-coarse crystalline vug-filling dolomite cement phase.

Interpretation

High-frequency sea level oscillation controlled the sedimentation of the Middle Anisian isolated carbonate platforms where cyclic successions of alternating shallow

subtidal, tidal flat and palaeosol facies were formed. Based on studies performed on partially dolomitized sections, synsedimentary dolomite formation and near-surface dolomitization were interpreted as the earliest stages of the dolomite genesis (Haas et al. 2014b). In the shallow subtidal lithofacies, fabric-selective porphyrotopic dolomite occurs in microbial fabric elements (clotted micrite, micrite nodules, microbial crusts, cortex of oncoids) suggesting organogenic Mg–Ca carbonate precipitation and/or selective replacement of the microbial high-Mg calcite (HMC) components. Organogenic Mg–Ca carbonate precipitation took place in the microbial tidal flat deposits. This primary carbonate precipitation was followed by progressive replacement of the carbonate sediments right beneath the surface. Pedogenic processes also resulted in dolomite formation. Dolomitic calcrete or dolocrete above the intertidal or truncated subtidal beds were developed in this way. In the partially dolomitized succession, intervals affected by complete fabric-destructive dolomitization were commonly found below subaerial exposure surfaces. This preferential stratiform dolomitization probably took place via reflux of evaporated sea water in a near-surface diagenetic setting.

Due to their dissimilar palaeogeographic settings, the burial history and related diagenetic conditions of the partially dolomitized and the pervasively dolomitized platforms were different (Haas et al. 2014b). In the latter case, after a short-term drowning episode platform conditions were restored giving rise to replacive dolomitization in a near-surface setting and in the course of burial. In contrast, in the case of the partially dolomitized platforms the relatively thin platform carbonate succession was covered by basinal deposits, preventing any intense circulation which is required for complete burial dolomitization. By the Late Norian, the Middle Triassic platform carbonates reached the intermediate burial realm. Medium-to-coarse crystalline dolomite occluded the newly opened fractures and vuggy pores.

Middle Triassic (uppermost Anisian–Ladinian) dolomitized platform carbonates

In the Middle Triassic, rift tectonics led to the formation of topographic highs with thick carbonate platform successions (Budaörs Formation; Figs. 4, 5) and coeval basins with limestone and tuff layers (Buchenstein and Füred Formations; Haas and Budai 1995).

Coeval carbonate platforms of various sizes are also known from the Southern Alps (De Zanche et al. 1993). In the Dolomites most of these platforms are pervasively dolomitized (Schlern = Sciliar Dolomite), but a few platforms (e.g. Latemar) were subjected only to partial dolomitization of various origins (Hardie et al. 1986; Blendinger 1997; Meister et al. 2013). Coeval platform carbonates (Wetterstein Formation) in the Northern Calcareous Alps and Western Carpathians were locally subjected to partial or complete dolomitization (Henrich and Zankl 1986; Lobitzer et al. 1990).

In the TR the platform succession consists of thick beds of massive dolomite; however, metre-scale cycles of alternating massive dolomite and thin-bedded/laminated dolomite lithofacies occur locally. These two lithofacies were subdivided into four fabric types, which occur systematically in accordance with the depositional succession (from bottom to top): (1) fabric-destructive dolomite and (2) bioclastic dolomite were found in the massive lithofacies, whereas (3) micritic dolomite and (4) microbial boundstone with fenestral pores characterize the thin-bedded/laminated one. These dolomite fabric types are composed altogether of four dolomite phases: aphanocrystals (1), fine replacive crystals (2), medium-to-coarse replacive crystals (3) and overgrowth cement (4).

The fabric-destructive dolomite and bioclastic dolomite are typified by medium and coarse crystals (Phase 3), and Phase 2 and Phase 4 are also present (Fig. 11a). In the bioclastic dolomite, the appearance and occurrence of the medium-to-coarse replacive crystals is heterogeneous. This dolomite (Phase 3) exhibits three crystal habits, which also differ in richness of solid inclusions and texture (Hips et al. 2015). They are as follows: dark brown, inclusion-rich anhedral mosaics (3a); lighter brown, isopachous, elongate, anhedral crystals (3b); and less inclusion-rich subhedral–anhedral crystals (3c). The dark brown, mosaic crystals (3a) are distributed in irregular mottles and unequally attached to the surface of altered bioclasts (Fig. 11a). Blue-light illumination of these mosaic crystals revealed bright green fluorescence. These features resemble a clotted micrite microfabric characteristic for the microbial deposits (e.g. Monty 1967, 1981; Défarge et al. 1996; Dupraz et al. 2004). Elongate dolomite crystals (3b) occur locally between the ghosts of bioclasts and in the primary intraparticle pores of skeletal fragments. These crystals exhibit undulose extinction, which moves into a uniform direction in sets of neighbouring crystals. The less inclusion-rich, subhedral–anhedral crystals (3c) occur mainly as a biomould pore-filling phase post-dating the dolomite silt infilling.

The microbial boundstone fabric type is characterized by the ubiquitous presence of aphanocrystalline dolomite (Phase 1; Fig. 11b, c). Arrangement of the submicron-sized crystals shows the characteristic appearance of calcimicrobes, (Fig. 7a, b, in Hips et al. 2015), clotted–spherular aggregates and bundles of prostrate threads. Clotted aggregates appear as spongy groundmass (Fig. 11c); accordingly they can hardly be sedimentary grains. Replacive fine crystals (Phase 2) occur in all four fabric types and are the main component of the micritic dolomite fabric type. Both the

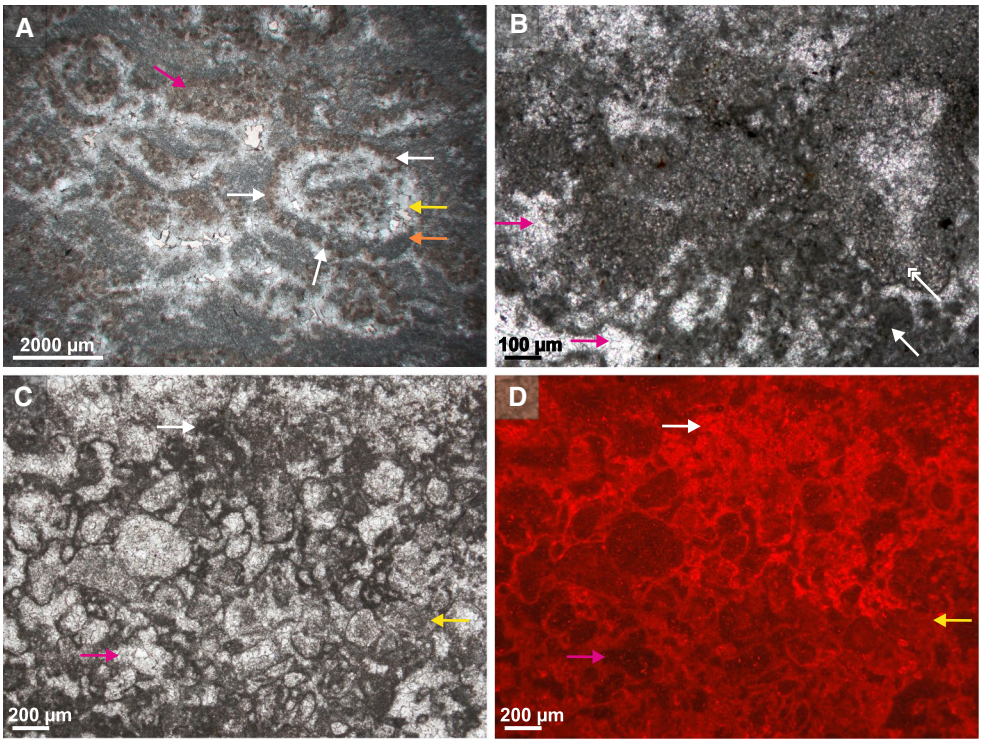

Fig. 11 Photomicrographs showing the dolomite fabrics (Budaörs Dolomite) (Hips et al. 2015). **a** Bioclastic dolomite fabric with ghosts of dasycladalean algae. *Dark brown*, inclusion-rich mosaics (Phase 3a; *white arrows*) delineate the biomoulds and form mottles (*pink arrow*). Dolomite silt at the bottom (*orange arrow*) and bands of less inclusion-rich mosaic crystals (Phase 3c and Phase 4; *yellow arrow*) filled the biomoulds. The *grey areas* consist of fine replacive crystals (Phase 2). **b** Framework structure of microbial boundstone fabric consists of aphanocrystals, which densely arranged in bushy clot clusters (*white arrow*) and irregular mottles (*double-headed white arrow*). Abundant uniform, oval-shaped globules (*double-headed white arrow*) are embedded among the dense, submicron-sized crystals. The pore network is filled by coarser cement crystals (*pink arrow*). **c** Nodular/reticulate lamina with aphanocrystals (Phase 1; *white arrow*), a mixture of aphanocrystals and fine crystals (Phases 1 and 2; *yellow arrow*) and medium crystals (Phase 3; *pink arrow*) in microbial boundstone fabric. **d** CL image of the same field of view shown in **b**. The aphanocrystals (*white arrow*) show dull red luminescence, the mixture of aphanocrystals and fine crystals (*yellow arrow*) show faint dull red luminescence and the medium crystals (*pink arrow*) show brighter spots in a non-luminescent background

aphanocrystalline and the finely crystalline dolomites display dull red luminescence (Fig. 11d). Fenestral pores of the microbial boundstone are filled by Phase 3 dolomite, which exhibits blotchy luminescence, and dolomite cement (Phase 4). Phase 4 cement forming a limpid overgrowth on replacive crystals was observed in every fabric type. These cement crystals exhibit dull red luminescence with fine non-luminescent subzones.

Stable isotope geochemistry

In the largest pores of the microbial boundstone, the medium and coarse crystals (Phases 3 and 4) were microdrilled together, but separately from the heterogeneous part of the rock. All other measurements were made on bulk rock powder samples. The $\delta^{13}C$ values of all analyses are similar, ranging between 2.2 and 3.9 ‰ (Fig. 6). The $\delta^{18}O$ values of dolomite crystals from large pores (−4.3 to −1.7 ‰) are depleted in ^{18}O relative to the values of the bulk samples. Bulk samples from microbial boundstone, micritic dolomite and bioclastic dolomite (potentially mixtures of all four dolomite crystal phases) yielded $\delta^{18}O$ values of 0.2–1.2 ‰. The fabric-destructive dolomite has $\delta^{18}O$ values in a wide range between −1.9 and 1.6 ‰.

Fluid inclusion petrography and microthermometry

Fluid inclusion data are available from two samples of microbial boundstone and from one sample of fabric-destructive dolomite (Poros 2011; Hips et al. 2015). The primary two-phase aqueous inclusions of the medium and coarse crystals (Phases 3 and 4) gave a similar range in the homogenization temperatures from the microbial boundstone (72 and 79 °C) and from the fabric-destructive dolomite (62 up to 83 °C). Entrapment temperatures of the fluid could not be calculated, but the homogenization temperature values still provide a valid measure of the minimum entrapment temperature (Goldstein and Reynolds 1994).

Only three inclusions were appropriate for salinity measurements. All of them were hosted by the inclusion-rich core of the dolomite crystals (Phase 3). The salinity values calculated from the final melting temperatures, assuming a NaCl–H_2O system, are 3.4, 3.8, and 6.4 NaCl eq. wt%.

Interpretation

Petrographic features of the bioclastic dolomite suggest the presence of three types of calcite precursors. The features of the dark brown, mosaic crystals (Phase 3a) indicate organogenic precursor crystals, likely aphanocrystalline high-Mg calcite (HMC), which was precipitated in microbial deposits rich in bioclasts. The lighter brown, elongate, anhedral dolomite crystals (phase 3b) exhibiting undulose extinction refer to fibrous calcite cement precursor (RFC; sensu Kendall 1985) precipitated after the formation of the aphanocrystalline phase. The features of the pore-filling, less inclusion-rich subhedral–anhedral crystals (Phase 3c) refer to a calcite cement precursor (CAL).

Comparative petrographic analyses of microbial boundstone (exhibiting microbial microfabrics) and bioclastic dolomite (including dolomitized organogenic calcite) provide circumstantial evidence suggesting that the aphanocrystalline dolomite (Phase 1) did not form via mimetic replacement. The precipitation of the aphanocrystalline dolomite is interpreted as having been occurred in deposits of microbial films and mat favouring/tolerating an increasing frequency of subaerial exposure in the upper intertidal setting. Therefore, the aphanocrystalline dolomite is interpreted as an organogenic primary dolomite precipitate.

The bulk rock $\delta^{18}O$ values of the microbial boundstone, micritic dolomite and bioclastic dolomite significantly differ from the much more negative values of the coarser crystalline replacive and cement dolomites. It can be assumed that the crystal association of the aphanocrystals (Phase 1) and the fine crystals (Phase 2) are more enriched in heavier oxygen isotopes than the solid phase mixture of all dolomite phases (cf. Banner and Hanson 1990)—since bulk rock samples include the ^{18}O-depleted crystal phases. The presence of mesohaline pore water is assumed during the precipitation of aphanocrystals (Phase 1; cf. Simms 1984) which likely occurred within buried, upper intertidal pustular mat deposits (cf. Allen et al. 2009; Abed et al. 2010). Although evaporite minerals do not occur in the formation, hypersaline condition likely determined the synsedimentary replacive dolomitization (Phase 2 crystals; Land 1983). This dolomitization phase was coupled with aragonite dissolution, and it post-dated the organogenic dolomite precipitation. This synsedimentary dolomitization occurred only in the peritidal caps of the shallowing-upward depositional units. Both peritidal processes (dolomite precipitation and replacement) were likely controlled by environmental factors in a semi-arid climate.

Those components of the platform succession that had not been dolomitized in the peritidal environment were replaced and cemented by medium and coarsely crystalline dolomite at elevated temperature in the intermediate burial realm (Hips et al. 2015, 2016). This process was not restricted to a particular depositional environment but affected the entire platform carbonate succession.

Carnian partially and selectively dolomitized reef limestone

A sea level rise, after the Carnian Pluvial Event, led to re-establishment and then progradation of the isolated carbonate platforms during the late Early Carnian highstand period. Massive carbonate bodies of reef facies were formed along the basinward margins of these platforms (Ederics Limestone) whereas cyclic peritidal successions were formed in the internal part of the platforms (Gémhegy Dolomite; Fig. 4). In the south-eastern part of the TR (Keszthely Mts.), the lower part of the reef limestone was locally subjected to low-grade partial dolomitization, whereas the upper part of the succession is usually entirely dolomitized. Multistage partial dolomitization of Carnian reef limestones, akin to that found in the Ederics Limestone, was reported from the Northern Calcareous Alps (Henrich and Zankl 1986).

The following lithofacies types were distinguished (Haas et al. 2014a): (1) Non-dolomitized to slightly dolomitized reef limestone characterized by boundstone and rudstone microfacies consisting of microbially encrusted calcareous sponges and colonial corals. A small amount of very finely crystalline dolomite aggregates and fine scattered dolomite rhombs, i.e. porphyrotopic dolomite, were found in the irregularly laminated and commonly filamentous micritic crusts (Fig. 12a). (2) Selectively dolomitized reef limestone with clusters of finely crystalline, planar-subhedral dolomite and medium-sized porphyrotopic dolomite crystals with inclusion-rich cores, occurring preferentially in microbial fabric composed by filamentous and clotted micrite (Fig. 12b). (3) Heavily dolomitized limestone showing remnants of precursor fabric elements (Fig. 12c). (4) Dolostone with ghosts of grains of the precursor limestone (Fig. 12d). (5) Fabric-destructive dolostone characterized by irregular mottles of aphanocrystals to coarse crystals (Fig. 12e). Dolostone characterized by unimodal medium, planar-subhedral crystals with inclusion-rich cores and clear rims is also included in this lithofacies.

In the selectively dolomitized and heavily dolomitized lithofacies, calcite-filled moulds, calcite bioclasts and vugs with isopachous calcite cement are common. Some

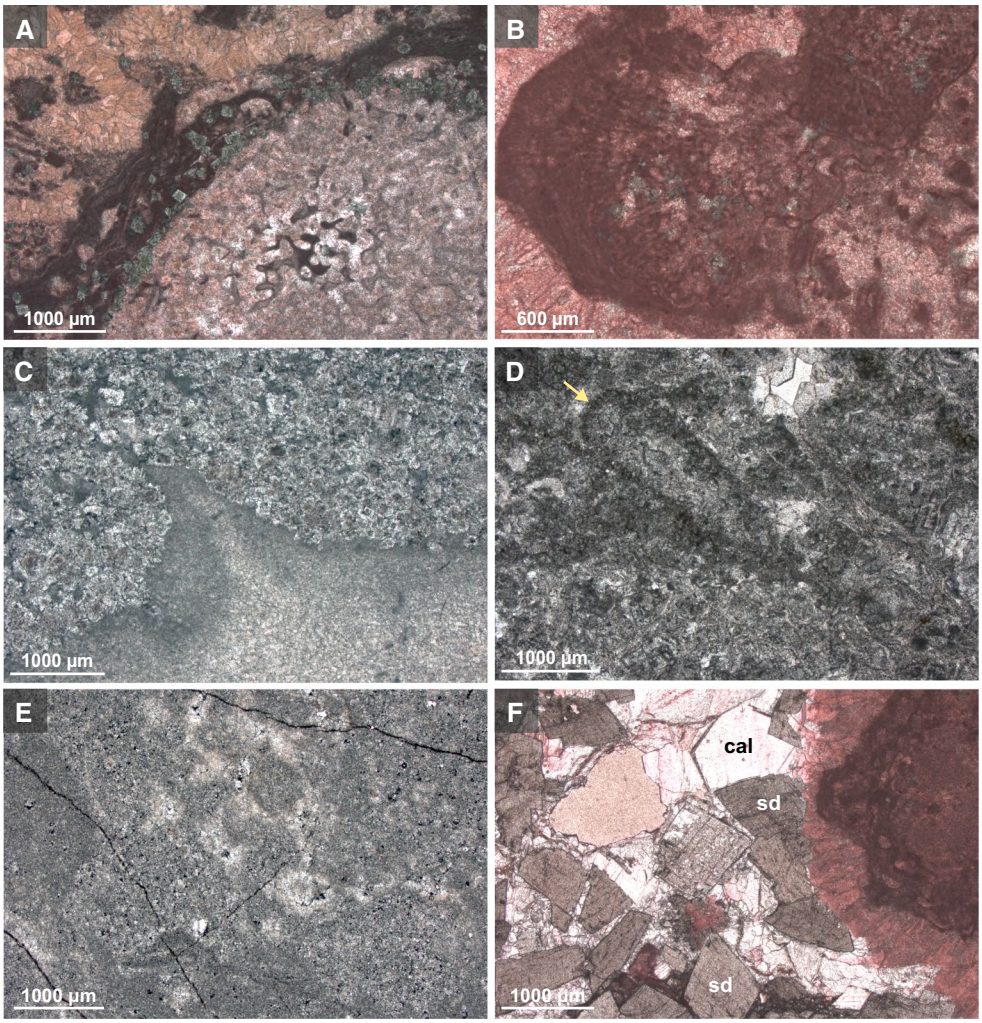

Fig. 12 Petrographic features of a partially dolomitized Carnian reef limestone (Ederics Formation), Well Bet-1, Balatonederics, Keszthely Mts. **a** Scattered porphyrotopic dolomite rhombs (planar-p) in filamentous microbial crust, 48.8 m. **b** Clusters and mottles of very finely crystalline dolomite and fine euhedral dolomite crystals in micritic components of the limestone, 64.5 m. **c** Mottles of fine-to-medium crystalline planar-subhedral dolomite with inclusion-rich cores and clear rim, 64.5 m. **d** Ghosts of bioclasts (*yellow arrows*) in finely to coarsely crystalline dolomite, 77.1 m. **e** Very finely to finely crystalline dolomite with aphanocrystalline mottles, 69.0 m. **f** Pore-filling saddle dolomite cement (*sd*), and coarsely crystalline calcite (*cal*) formed as a cement and via calcitization of the dolomite cement, 129.7 m. Stained thin sections: **a**, **b**, **e**, **f**

of the vuggy pores crosscut partially dolomitized calcimicrobes and microbial crusts. No porphyrotopic dolomite was found, whether in isopachous cement, in calcite bioclasts or calcite-filled biomoulds. Accordingly, the mould and vug-creating dissolution, and the precipitation of the mould- and vug-filling calcite cement post-date the very finely crystalline dolomite generation. In some cases the bioclasts and calcite-filled biomoulds are completely or partially replaced by fine-to-medium crystalline planar-subhedral and/or nonplanar-anhedral dolomite. Therefore, this generation of replacive dolomite post-dates the mould and vug-filling calcite cement. Completely dolomitized segments with ghosts of original sedimentary fabric elements, and replaced fibrous cement, as well as completely fabric-destructive dolomite may have formed, either during this stage or subsequently, but prior to the precipitation of medium crystalline dolomite and saddle dolomite cement representing the last dolomite phase (Fig. 12f). The latter phases are usually present in fractures or in the internal, remnant parts of growth-framework pores and in intergranular or vuggy pores in every lithofacies type, from reef limestone to completely dolomitized rock types.

Stable isotope geochemistry

The $\delta^{13}C$ and $\delta^{18}O$ values of the samples taken from various fabric elements (micrite, microbial crust, and calcite cements) of the non-dolomitized or slightly dolomitized

reef limestone lithofacies ($\delta^{13}C$: 3.0–3.2 ‰; $\delta^{18}O$: −3.8 to −2.7 ‰; Fig. 6) are within the range expected for calcite precipitated in equilibrium with Carnian seawater (Korte et al. 2005). Porphyrotopic dolomite was sampled and measured separately and gave values of 3.7 ‰ for $\delta^{13}C$ and −3.5 ‰ for $\delta^{18}O$. Both $\delta^{13}C$ and $\delta^{18}O$ values of the finely crystalline dolomite measured in strongly dolomitized rock types are similar to those of the reef limestone but show a slightly wider range ($\delta^{13}C$: 2.7–4.1 ‰; $\delta^{18}O$: −4.3 to −2.0 ‰). Values of the dolomitized fibrous calcite cement ($\delta^{13}C$: 3.3–4.0 ‰; $\delta^{18}O$: −3.4 to −2.9 ‰) are within the field of finely crystalline dolomite. The values representing medium crystalline dolomite and coarsely crystalline saddle dolomite are typified by a narrow $\delta^{13}C$ range (2.4–3.1 ‰) but a wide $\delta^{13}O$ range (−9.1 to −5.3 ‰).

Fluid inclusion petrography and microthermometry

Fluid inclusion studies were carried out on saddle dolomite samples. Primary fluid inclusions in saddle dolomite crystals are 1–10 μm in size and their shape is irregular. The inclusions are commonly present along growth zones. They are two-phase (liquid–vapour) inclusions, when determinable, with constant phase ratios (L:V = 90:10–95:5). Several secondary inclusions were also observed along cleavage planes. Microthermometry was carried out on the primary two-phase aqueous inclusions. The inclusions homogenized into liquid phase. Measured homogenization temperatures fall between 60 and 98 °C. The vapour phase of the inclusions usually did not reappear during cooling to room temperature or below; therefore, it was not possible to measure the final melting temperature.

Interpretation

A series of diagenetic processes led to the partial dolomitization of the Carnian reefs. The diagenesis of the submarine reef included biological encrustation of the skeletal components, microbially mediated and the abiotic cementation, bioerosion and mechanical destruction of the build-ups. In this stage, Mg-rich carbonate (HMC, VHMC) microaggregates selectively formed in microbial mats and crusts. The very finely crystalline aggregates represent the earliest dolomite generation. It was succeeded by the formation of the euhedral crystals around the tiny dolomite aggregates, which acted as the nuclei for the small dolomite rhombs (cf. Choquette and Hiatt 2008). Then, in the course of burial, the individual crystals merged to dolomite mottles and the extension of the mottles led to the formation of finely crystalline replacive dolomite. The Carnian reef carbonates reached 1–1.5 km burial depth by the Late Norian. The negative $\delta^{18}O$ values measured on medium-to-coarse crystalline fracture and pore-filling dolomite cement indicate elevated temperature of the dolomitizing fluid. This is in accordance with the morphology of the crystals (saddle dolomite forms above 60 °C, Spötl and Pitman 1998) and the fluid inclusion data that gave minimum 60 °C for the parent fluid.

Carnian–Norian dolomitized and partially dolomitized platform carbonates

In the Late Triassic, a ca 2.5-km-thick platform carbonate succession was formed. The lower part of this cyclic, peritidal succession is completely dolomitized (Gémhegy Dolomite and Fődolomit Formations; Figs. 4, 5). There is a gradual transition between the dolostone (Fődolomit Formation) and the overlying limestone (Dachstein Limestone). The transitional interval (Fenyőfő Member) is characterized by alternation of entirely dolomitized, partially dolomitized and non-dolomitized segments (Balog et al. 1999; Haas and Demény 2002).

Gradual transition between the Hauptdolomit and the internal platform facies of the Dachstein Limestone was locally observed also in the Northern Calcareous Alps (Mandl 2000), although detailed studies on the transitional interval have not been performed. The characteristics of the Dolomia Principale (Frisia 1994; Meister et al. 2013) are very similar to those of the Fődolomit Formation; however, due to a sea level fall, there is no marine record of the latest Norian in the Southern Alps. Therefore, study of the gradual climate change signals is not possible in that area (Berra et al. 2010; Haas et al. 2015).

The 1- to 5 m-thick cycles are mostly bounded by nearly flat or slightly uneven bedding planes (Lofer cycles—cf. Fischer 1964, 1991). The entirely dolomitized succession, exhibiting depositional fabrics, is made up of an alternation of wackestone–packstone–grainstone beds with marine biota (Lithofacies C; Lf C) and stromatolite beds (Lithofacies B; Lf B). The cycles are locally capped by a centimetre to tens of centimetres-thick, laminar, brecciated and rarely pisolitic pedogenic crust (Lithofacies A; Lf A—Balog et al. 1999). The transitional unit is composed of an alternation of these lithofacies types, but additionally, a reddish or greenish lithoclastic, argillaceous carbonate layer (Lf A) may appear above the disconformity surface.

In the completely dolomitized formations, the stromatolite beds consist of clotted micrite and fenestral pores filled by fine-to-medium crystalline dolomite cement (Fig. 13a, b). In the Lf C beds, the degree of fabric preservation varies between good fabric preservation (Fig. 13c, d) and complete fabric destruction. The fabric-destructive dolomite is usually very finely to finely crystalline, exhibiting predominantly planar-subhedral texture. The crystals have inclusion-rich cores and limpid rims showing mottled and dull red CL, respectively.

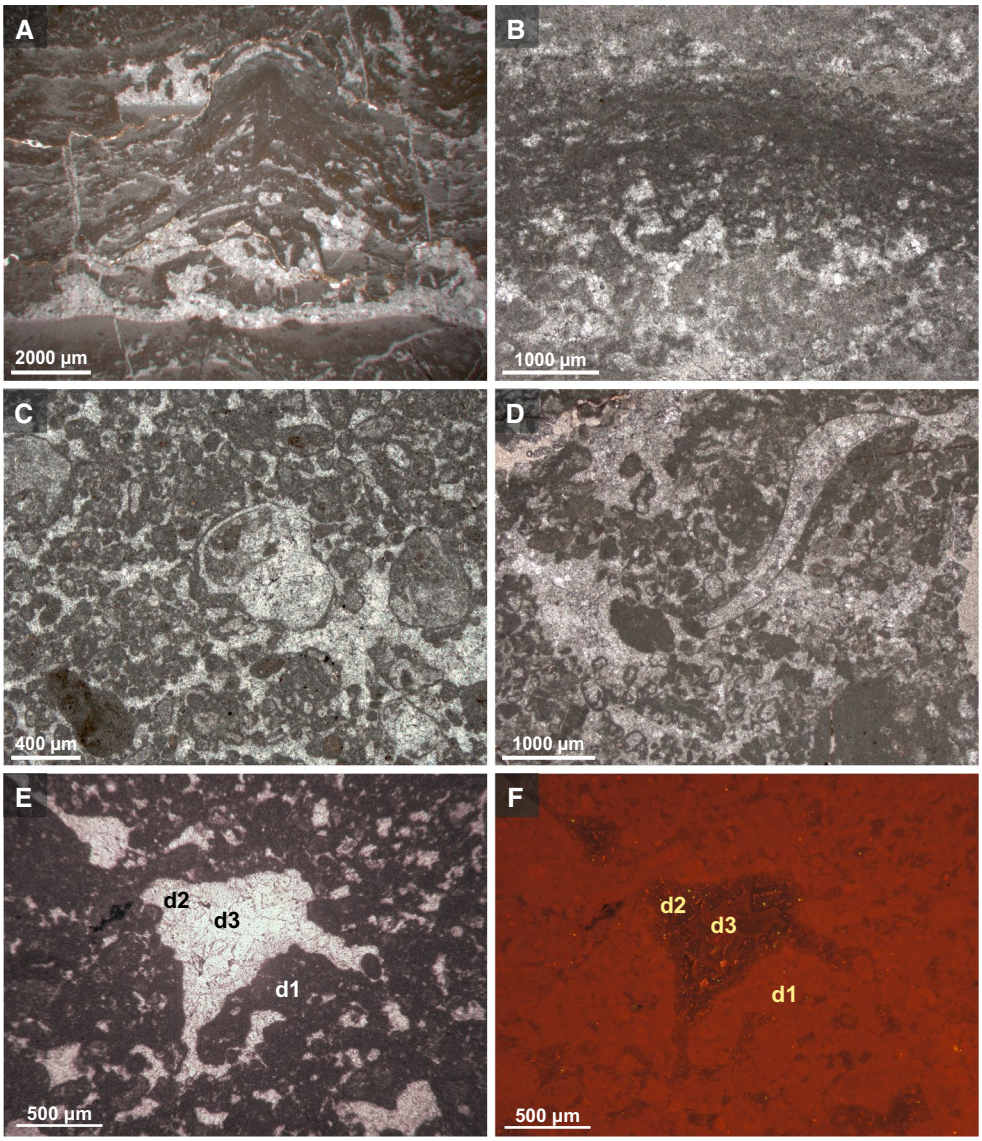

Fig. 13 Common fabrics of the Gémhegy Dolomite and Fődolomit Formation. **a** Lf B—millimetre-sized domical structure in stromatolite. Upper part of the Fődolomit Formation, Csákánykő Quarry, Vértes Mts. **b** Undulating laminated and clotted micritic microfabric of Lf B. Middle part of the Fődolomit Formation, Horogvölgy section, Vértes Mts. **c** and **d** Peloidal grainstone with cement-filled moulds of skeletal fragments of bivalves and gastropods. Lower part of the Fődolomit Formation, Aranyosvölgy Quarry, Bakony Mts. **e** Microbial boundstone with fenestral pores. Lower part of the Fődolomit Formation, Aranyosvölgy Quarry, Bakony Mts. **f** CL image (overexposed) of the field of view shown in **e**. Aphanocrystalline dolomite has dull red luminescence (*d1*) and pores are lined by inclusion-rich, fine-to-medium crystalline dolomite with mottled luminescence (*d2*), which is overgrown by a dull red, zoned dolomite cement (*d3*)

Very fine-to-medium crystalline dolomite occurs in the intergranular pores in the Lf C beds, as well as in larger vuggy pores and fractures in both the microbial beds (Lf B) and Lf C beds. This dolomite phase is always rich in inclusions and it is commonly overgrown by medium-to-coarse crystalline clear dolomite cement (Fig. 13e, f).

In the transitional interval, both fabric-selective and non-selective dolomite types were observed. When fabric-selective the clotted micrite of Lf B is usually dolomite; the fenestral pores are fringed by finely crystalline dolomite and usually filled by calcite (Fig. 14a), whereas scattered dolomite crystals occur in the micrite matrix of Lf C (porphyrotopic texture; Fig. 14b, c). When not fabric-selective the dolomite crystals occur in irregular mottles (Fig. 14d).

Stable isotope geochemistry

There is no obvious correlation between the degree of fabric preservation and the isotope values, nor are differences in the sedimentary fabric reflected in the isotope

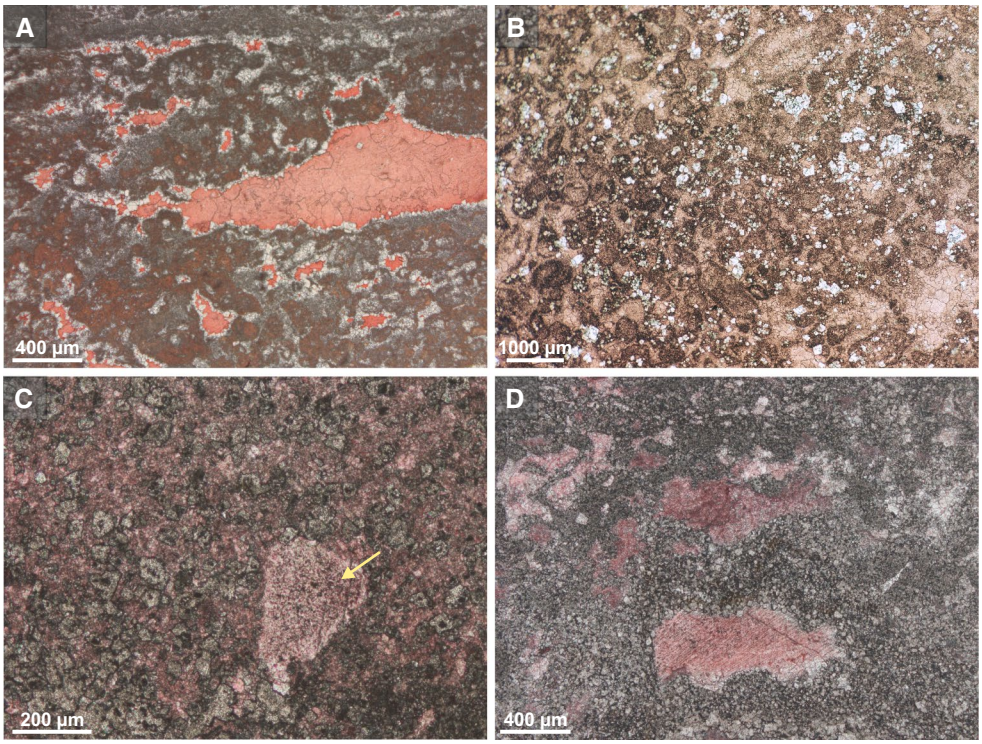

Fig. 14 Characteristic fabrics of the transitional interval (Fenyőfő Member and basal part of the Dachstein Limestone (*s.s.*)). **a** Stromatolite—Lf B. Aphanocrystalline dolomite boundstone. The fenestral pores are rimmed by finely crystalline clear dolomite cement followed by calcite cement. Basal part of the Dachstein Limestone (*s.s.*) well Po-89, 412.0 m, Bakony Mts. **b** Partially dolomitized peloidal, bioclastic grainstone—Lf C. Fenyőfő Mb, well Po-89, 467.5 m, Bakony Mts. **c** Partially dolomitized peloidal wackestone—Lf C. The echinoderm fragment (*yellow arrow*) was not affected by dolomitization. Fenyőfő Mb, Epöl Quarry, Gerecse Mts. **d** Heavily dolomitized limestone—Lf C. Fenyőfő Mb, Epöl Quarry, Gerecse Mts. Stained thin sections

values. The $\delta^{18}O$ values of both the Gémhegy Dolomite and the Fődolomit Formations are scattered within a narrow range from 0.5 to 3.1 ‰. These values are very similar to those reported from the early dolomite phases of the equivalent South Alpine Dolomia Principale (0.6–3.0 ‰; Frisia 1994; Meister et al. 2013). The $\delta^{18}O$ values for the Fenyőfő Member are comparable with the transitional features of this unit between the Fődolomit and the Dachstein Limestone (Fig. 6; for further details see Haas et al. 2015). The $\delta^{13}C$ values range from 1.2 to 3.8 ‰, within the range of Carnian to Norian sea water (Korte et al. 2005). The $\delta^{18}O$ values of cements are always more depleted in ^{18}O compared to the replacive dolomite values; the difference is 1–5 ‰. The $\delta^{13}C$ values of the dolomite cement do not significantly differ from those of the replacive dolomite.

Interpretation

Synsedimentary and near-surface diagenetic processes led to the formation of dolomite in the wide internal zone of the Late Triassic carbonate platforms, where high-frequency sea level oscillations resulted in the deposition of unconformity-bounded, metre-scale peritidal cycles (Haas et al. 2015). No near-surface dolomite was found in the coeval deposits of the permanently subtidal external platform belt (Remetehegy Limestone Mb of the Dachstein Limestone; Figs. 4, 5). Thus, the recurring subaerial exposure in the supratidal zone appears to be an important controlling factor of the near-surface dolomite formation.

Selective occurrence of dolomite in the clotted micrite microfabric of the laminated microbial deposits in the Fenyőfő Mb suggests synsedimentary organogenic precipitation of Mg–Ca carbonates (VHMC), which may have been the metastable precursor phases to dolomite. Dolomitization of the subtidal facies took place via reflux of evaporated sea water during longer-term subaerial episodes. The conditions of near-surface dolomitization were likely re-established during the successive exposure events, which resulted in the completion of the dolomitization of the subtidal facies.

The sea-level-controlled and unconformity-bounded cyclic facies pattern did not change significantly in the study area during the Late Triassic. Therefore, the upward decreasing dolomite content through the transitional part up

to the overlying limestone suggests climatic control rather than a change in the depositional setting. The increasing humidity probably led to gradually decreasing intensity and finally almost complete cessation of the near-surface dolomitization processes by the latest Triassic.

In the course of burial an extensional tectonic regime prevailed from the latest Norian to Middle Jurassic, leading to formation of fractures later cemented by dolomite. Relatively low $\delta^{18}O$ values of these dolomite cements indicate elevated temperature.

Carnian–Norian dolomitized slope and basinal carbonates

During the Late Triassic spreading stage, fault-controlled extensional basins developed near the platform margin. Biogenic silica and organic matter-rich carbonates were deposited in the basins. Cherty dolostone occurs in the lower part of the succession, progressing into cherty limestone upsection (Mátyáshegy Formation in the Buda Mts, Csővár Limestone Formation in the Csővár Hills, Danube-East blocks; Figs. 2, 4; Haas 1994, 2002; Haas et al. 1997).

Thick-bedded (10–30 cm) dolostone contains grey or brown 5- to 10-cm-sized chert nodules and/or 1- to 2-cm-sized angular chert clasts. In the Buda Mts, alternation of dark and medium grey laminae was commonly observed in the upper part of the dolostone succession. The crystal size moderately or significantly varies from fine to coarse (Fig. 15a). The medium-to-coarse saddle dolomite occurs as a replacive phase as well as a pore-filling cement. In the laminated dolomite, aphanocrystalline clots and peloids are minor components that are arranged into discontinuous bands (Fig. 15b). Very fine-to-fine dolomite crystals occur in the partially dolomitized limestone upsection.

The completely dolomitized part of the formation is characterized by variously sized mottles resembling multiphase breccia fabric (Figs. 6, 7, 8 in Hips et al. 2016). The coarser crystalline mottles commonly cut across the boundary of fine and medium crystalline mottles. The latest phase is limpid saddle dolomite cement precipitated within a fracture-network. No preserved sedimentary components or sedimentary fabric can be recognized inside the mottles/breccia clasts. The fine-to-medium, subhedral–anhedral crystals have blotchy dull red luminescence, whereas the rhombohedral medium crystals display a core and growth zones of variously dull red luminescence. The medium and coarse anhedral saddle dolomite crystals show dull red blotchy luminescence, or they have a blotchy core and a faint red rim. The coarse saddle dolomite crystals exhibit variously intense dull red growth zones with a brighter red subzone under CL.

Stable isotope geochemistry

Only the fracture-filling saddle dolomite cement from large pores was measured separately; otherwise, bulk rock samples were analysed. The $\delta^{13}C$ values of all samples are similar, ranging between 2.2 and 3.3 ‰ (Fig. 6). The $\delta^{18}O$ values of the coarse saddle dolomite (ranging between −9.1 and −6.0 ‰) are much more depleted in ^{18}O relative to those of bulk samples of fine-to-medium crystalline dolomite (−1.3 to 2.1 ‰). The bulk rock values, representing all phases together, yielded a $\delta^{18}O$ range from −5.4 to −1.3 ‰.

Fluid inclusion petrography and microthermometry

Primary aqueous fluid inclusions of the medium crystalline replacive subhedral dolomite crystals and the saddle dolomite cement were analysed. In the core of the subhedral crystals, isometric primary fluid inclusions are

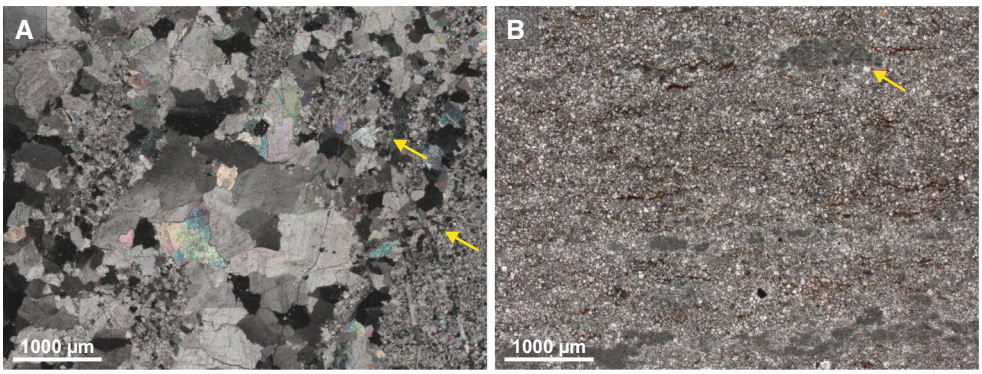

Fig. 15 Photomicrographs of Upper Triassic dolomite (Mátyáshegy and Csővár Limestone Formations). **a** Mottles with irregular boundaries consist of crystals of various sizes. The transition is commonly gradual between the mottles as shown by the gradually increasing crystal size (*arrows*), but sharp boundaries are also visible. Well Csv-1, 638.0 m, crossed polars. **b** Finely crystalline dolomite with aphanocrystalline components occurring in lamina (*arrow*) and with scattered medium subhedral crystals. Remnants of organic matter (*brown*) occur in intercrystalline pores and along solution seams; well Vh-1, 242.3 m

also present from 1 to 5 μm in size. They are all monophase liquid inclusions, implying that the precipitation of the mineral occurred below 50 °C (Goldstein and Reynolds 1994). Fluid inclusions are also present in the core and along growth zones of the saddle dolomite crystals. Microthermometry was carried out on the primary two-phase inclusions of saddle dolomite crystals. The measured homogenization temperature values range between 72 and 108 °C. The homogenization temperature values provide a reasonable approximation of entrapment temperatures in this case, given the relatively low salinity of the fluid (Goldstein and Reynolds 1994). Five final melting temperatures were obtained, which range between −1.8 and −1.1 °C. These values are equivalent to a salinity range from 1.9 to 3.1 NaCl eq. wt%, assuming a NaCl–H_2O system.

Interpretation

Fine-to-medium, subhedral–anhedral crystals were interpreted as having been formed via a replacive process (Hips et al. 2016). The primary monophase aqueous inclusions of the subhedral crystals indicate formation below 50 °C (cf. Goldstein and Reynolds 1994). The 70 °C minimum entrapment temperature of the saddle dolomite implies elevated temperature of the fluid compared to that of the replacive fine-to-medium crystals. The negative $\delta^{18}O$ values of the saddle dolomite crystals are also in accordance with these results (cf. Land 1983). The paragenetic sequence, the isotopic values and the fluid inclusion data indicate that the various dolomites were formed by the same fluid at different temperatures rather than by various fluids of different compositions. Petrographic study revealed that the peculiar breccia fabric is not inherited from the precursor carbonates, but was formed during the dolomitization process, possibly under the influence of repetitive seismic shocks. As a result of rising temperature of the dolomitizing fluid, the precursor carbonates were replaced by coarser and coarser and eventually by saddle dolomite that also precipitated as cement. Bed-parallel stylolites in the dolostone suggest that dolomitization took place in intermediate burial realm prior to the onset of chemical compaction.

The geologic setting and palaeontological data indicate that the elevated blocks, located among the fault-related extensional basins, were subjected to subaerial exposure in the Rhaetian (Haas et al. 2000, 2010). Under humid climate conditions, meteoric water lenses were established within these blocks. Mixing of the deeply circulated freshwater with the fault-channelled ascending fluid may have been possible in this setting, which in turn could explain the low salinity of the parent fluid.

Discussion

Dolomite-forming processes

Comprehensive studies of dolomite-bearing formations of the TR revealed that dolomitization is never a single event but the result of series of diagenetic processes. It is of crucial importance to determine the main phase of the dolomitization that can be defined as the stage of transformation of the main mass of the $CaCO_3$—dominated sediments or rocks into dolostone. This main phase may have been preceded by phases of protodolomite/dolomite-forming processes usually resulting in small amounts of dolomite. In some cases, mostly in the partially dolomitized formations, traces of the early incipient dolomitization are preserved. Although the amount of the synsedimentary (penecontemporaneous) Ca–Mg carbonate phases was generally small, the dolomite, which formed via transformation of a very high-Mg calcite (VHMC) precursor, probably played an important role during subsequent dolomitization (Machel 2004; Gregg et al. 2015). The main dolomitization phase was commonly followed by dolomite cement precipitation in open pores and fractures in rock-buffered settings and/or in hydrothermal systems. In the course of the multiple dolomitization processes, various dolomite-forming mechanisms were in operation (Fig. 16).

Organogenic dolomite formation

Studies in various modern natural environments—mostly in microbial mat or organic-rich carbonate deposits, located in peritidal settings—pointed out the presence of VHMC or protodolomite (Wright 1990; Vasconcelos et al. 1995; Wright 2000; Mazzullo 2000; Wright and Wacey 2005; Dupraz et al. 2009; Bontognali et al. 2010). Laboratory experiments demonstrate the possibility of VHMC nucleation in microbe-secreted extracellular polymeric substances (EPS; Vasconcelos et al. 1995; Sánchez-Román et al. 2008; Bontognali et al. 2008, 2010; Spadafora et al. 2010). However, VHMC was also produced in the laboratory at ambient temperature without microbes (Gregg et al. 2015). Abiotic precipitation of dolomite within organic matter, with a high density of carboxyl groups has been demonstrated (Roberts et al. 2013); furthermore, polysaccharide-catalysed and dissolved sulphide-catalysed precipitation of VHMC were also pointed out (Zhang et al. 2012a, b). VHMC is commonly regarded as the precursor to ordered dolomite (e.g. Zhang et al. 2015) although there is no unambiguous evidence for this (Gregg et al. 2015).

Distinction of dolomite formed primarily as organogenic mineral from those that mimetically replaced the organogenic calcium carbonate precursor is extremely difficult in fossil microbial mat deposits. Additionally, in the case of

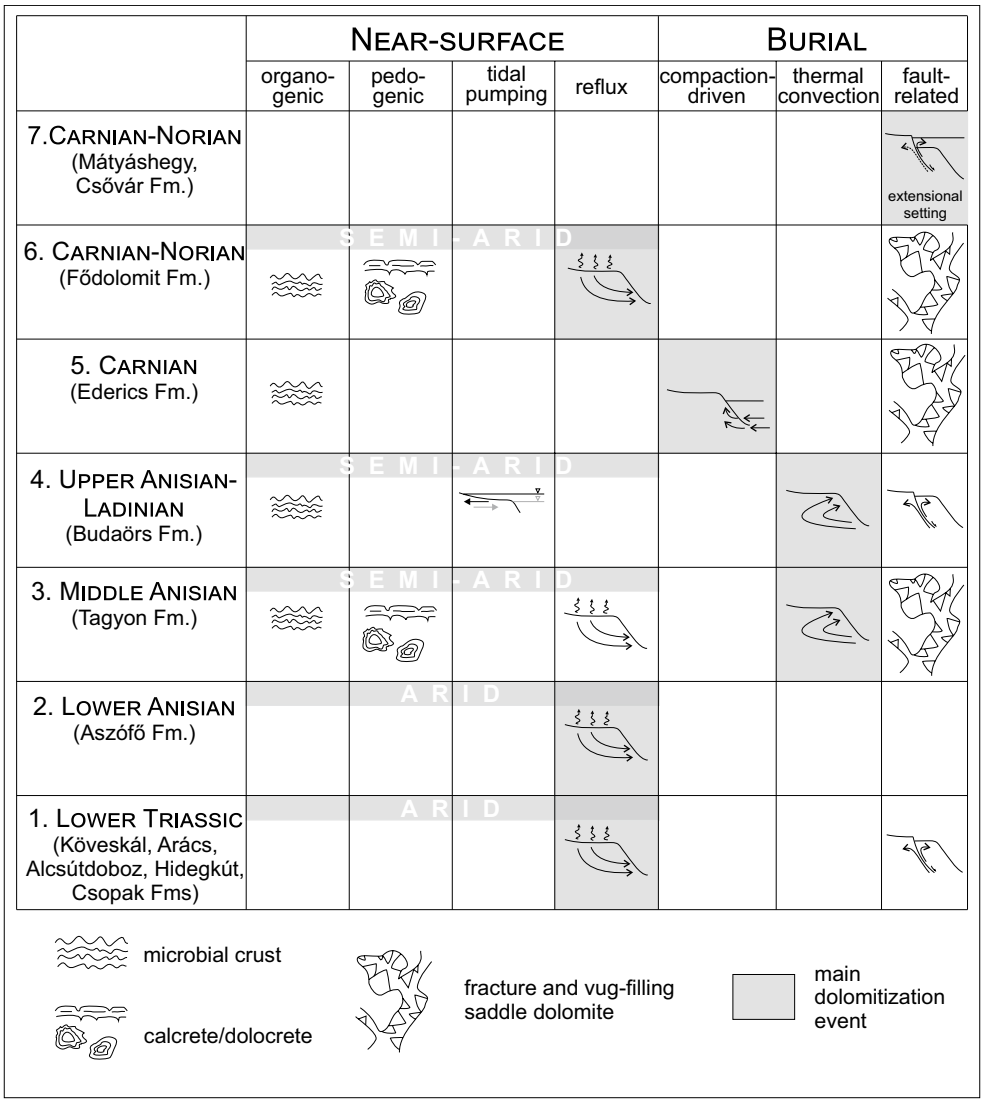

Fig. 16 Schematic diagram showing the dolomite-forming processes interpreted for the studied formations in the Transdanubian Range

ancient rocks, it is not possible to determine whether disordered protodolomite or ordered dolomite precipitated primarily (cf. Wenk et al. 1993). In the studied Triassic formations, petrographic analyses provide circumstantial evidence for primarily precipitated organogenic protodolomite/dolomite (Haas et al. 2014a, b, 2015; Hips et al. 2015).

Organogenic dolomite formation, was interpreted both in subtidal and tidal flat settings. In the case of the subtidal setting the concept was based on petrographic evidence from two of the studied formations. Textures characteristic of selective dolomitization of microbial fabric elements was observed in Carnian reef limestone. Clusters of fine crystals and scattered medium dolomite rhombs occur preferentially in filamentous crusts and in clotted micrite, whereas they are missing from calcite skeletal fragments, and from calcite cement phases. In the subtidal beds of Middle Anisian cyclic shallow platform deposits, dolomite rhombs of similar size were found in microbial crusts covering skeletal grains, in the cortex of oncoids, and in clotted micrite nodules (Haas et al. 2014b). It is supposed that VHMC along with HMC crystals nucleated within microbial organic matter (Haas et al. 2014a, b). The precipitation of organogenic minerals was followed by their stabilization and enlargement via a series of successive processes. This stabilization process was described from many limestones with HMC components (e.g. skeletal grains, or cement) whereby HMC is converted to LMC and microdolomite (e.g. Lohmann and Meyers 1977; Leutloff and Meyers 1984).

Organogenic dolomite formation in tidal flat setting was assumed for microbial deposits. The formation of the

primary precipitates (HMC, VHMC) was succeeded by recrystallization and related cation ordering. In the case of the Carnian–Norian platform carbonates, a definite relationship between the microbial deposits and the synsedimentary dolomite-forming processes was inferred in the transitional interval between the entirely dolomitized and selectively dolomitized parts of the succession (Haas et al. 2015). In this interval, the tidal flat microbialite beds have significant dolomite content, whereas the subtidal beds are either selectively dolomitized to various degrees or non-dolomitized. Fabric-selective occurrence of dolomite crystals in the laminated microbial deposits suggests organogenic precipitation of Mg–Ca carbonates. In the stromatolite beds, the clotted micrite is predominantly composed by dolomite whereas the fenestral pores are generally rimmed by dolomite cement post-dated by mosaic calcite cement (Haas 1995). The clotted micrite usually contains small amounts of dolomite in the stromatolite beds even in the lower part of the otherwise non-dolomitized Dachstein Limestone (i.e. in an interval directly above the transitional Fenyőfő Member). In the same interval, rip-up clasts derived from dolomitic stromatolite are common in the basal part of non-dolomitized subtidal beds (Haas et al. 2015). These observations also support synsedimentary dolomite formation.

In the pervasively dolomitized Anisian–Ladinian platform carbonates, two dolomite fabric successions representing low- and high-energy tidal flat settings were distinguished (Hips et al. 2015). In the succession formed in the low-energy setting, aphanocrystalline organogenic dolomite precipitation prevailed in the uppermost part of the deposits, followed by synsedimentary replacive dolomitization triggered by tidal pumping. In the succession formed in high-energy setting, thick beds of fabric-destructive dolomite alternate with thin layers of bioclastic dolomite and overlying microbial boundstone. According to the interpretation based on petrographic features of the dolomite textures, organogenic dolomite precipitated in the microbial boundstone, whereas organogenic calcite (HMC) formed in the bioclastic dolomite. In the microbial boundstone, the aphanocrystals form calcimicrobes and clotted micrite. In the bioclastic dolomite, the supposed HMC was partly replaced by fine dolomite crystals in a peritidal environment and partly by dark brown, medium crystalline, mosaic crystals during further burial. It is therefore assumed that the aphanocrystalline phase in the microbial boundstone formed primarily whereas the HMC in the bioclastic dolomite was replaced non-mimetically.

Pedogenesis-related dolomite formation

Example of pedogenesis-related dolomite formation was found in the Middle Anisian cyclic platform succession (Haas et al. 2014b). The sea level lowering resulted in erosion and pedogenesis, including dissolution of aragonite bioclasts, e.g. dasycladalean algae, via reaction with meteoric fluid. On the subaerially exposed carbonate platforms, under semi-arid climatic conditions, carbonate soils, i.e. calcretes/dolocretes, developed (Haas et al. 2012, 2014b). Thin pedogenic crusts were also encountered in the Upper Carnian to Norian platform succession both in the entirely dolomitized and in the partially dolomitized transitional sections (Balog et al. 1999; Haas 2004; Haas et al. 2015).

In the genesis of the calcretes/dolocretes, rainfall is the critical factor. Carbonate accumulates in soils with moisture deficit, i.e. the carbonate precipitated in the dry season is not leached away during the wet season (Wright 1994; Alonso-Zarza and Wright 2010). However, the duration of the subaerial exposure, the substrate lithology, the topography and the vegetation also influence the characteristics of the calcrete/dolocrete (Wright and Tucker 1991). Pedogenesis could be associated with dolomite formation, which includes precipitation and/or mineral replacement, leading to the development of dolocrete horizons (Alonso-Zarza et al. 1998; Wright 2007). There are only a few case studies for pedogenic dolomite-forming in the coastal belt on top of peritidal deposits. The shallowing-upward cycles in the Lower Carboniferous ramp successions of the northern Rocky Mountains could be analogous to the studied Triassic succession. The metre-scale cycles are composed of ooid grainstone, pelleted dolomite or laminated microbial deposits which may be capped by a mottled dolosilt palaeosol layer (Elrick and Read 1991). Dolomitic palaeosols punctuating a shallow marine–lagoonal argillaceous dolomudstone succession was recognized in the Devonian of the Holy Cross Mountains, Poland (Narkiewicz and Retallack 2014).

Dolomitization via tidal pumping

Tidal pumping across the tidal flat is relatively short-lived but it is regarded as an efficient flow mechanism for alteration of surficial intertidal sedimentary veneers (Carballo et al. 1987; Mazzullo et al. 1987; Gregg et al. 1992; Teal et al. 2000). The Anisian–Ladinian dolostone provides an example for dolomitization of intertidal deposits driven by tidal pumping (Hips et al. 2015). Such synsedimentary dolomitization coupled with aragonite dissolution post-dated the aphanocrystalline organogenic mineral precipitation and resulted in the formation of fine dolomite crystals. A facies shift as well as seasonal variation influenced the saturation state of the pore fluid with respect to various carbonate minerals that led to alteration processes of calcium carbonate within the mat deposits. The tidal pumping-related dolomitization may have played some role in the dolomitization of the

peritidal deposits of the Carnian–Norian platform successions as well.

Reflux dolomitization

During the Triassic green-house regime the low amplitude/high-frequency sea level fluctuation led to accumulation of metre-scale cycles with tidal flat caps on the carbonate platforms, and the sea level drops were associated with limited erosion only. In the arid to semi-arid regions, due to the intense evaporation, mesohaline/hypersaline water occurred in the tidal flat ponds and brine infiltrated into the unconsolidated subsurface deposits. The high-salinity water flowed downward and seaward through the carbonate sediment which led to replacive dolomitization (Adams and Rhodes 1960; Read and Horbury 1993; Whitaker and Smart 1993; Purser et al. 1994; Lucia and Major 1994; Jones and Xiao 2005).

Replacive non-ferroan dolomite, found within the Lower Triassic shallow marine, mixed siliciclastic–carbonate rocks, may provide an example for the near-surface reflux process. Dolomitization of the evaporite-bearing tidal flat and the inner ramp deposits was very likely the result of such high-density fluid circulation. In the case of the Lower Anisian dolostone, the evaporite-bearing carbonate deposition took place in a restricted, high-salinity inner ramp environment, which was gradually covered by the prograding tidal flat. Only a minor amount of evaporite was found in the supratidal beds, which indicates a less dry, semi-arid climate (Haas et al. 2012). Therefore, this deposit cannot be regarded as a typical sabkha succession; rather, it was formed in a moderately dry tidal flat environment. Complete dolomitization of the peritidal carbonates can be interpreted as a result of the reflux of mesohaline/hypersaline fluids.

In the partially dolomitized Middle Anisian succession, the fabric-destructive dolomite segments, which commonly occur below calcrete/dolocrete horizons, are interpreted as a result of reflux of evaporated sea water through the high-permeability calcarenite precursor sediment (Haas et al. 2014b). Reflux in a near-surface setting caused the pervasive dolomitization of the Carnian–Norian platform succession (Balog et al. 1999; Haas 2004; Haas et al. 2015). Semi-arid climate is supposed for this long interval, but the lack of evaporites suggests that it was less dry than in the Early Anisian (Haas et al. 2012). During the high-frequency sea level oscillations, falling sea level resulted in progradation of the tidal flats, and intense evaporation under semi-arid climatic conditions. This led to the formation of brines in shallow pools of the supratidal zone and coastal plain. Reflux of the evaporative sea water resulted in the dolomitization of the calcareous components of the stromatolite beds, and the predominantly wackestone subtidal beds. Increasing humidity in the early Late Norian resulted in decreased intensity of evaporation and thus, lower effectiveness of circulation. This is reflected in the partial dolomitization of subtidal beds as opposed to earlier complete dolomitization under more arid climatic conditions (Haas et al. 2015).

Compaction-driven dolomitization

Fluid flow as a result of dewatering of adjacent coeval clay-rich basinal deposits may cause local dolomitization at the platform margins (Illing 1959; Gawthorpe 1987). Although published case studies are rather limited (Morrow 1982; Land 1985; Machel and Anderson 1989), the local and usually low to moderate-grade dolomitization is in accordance with this model. In the partially dolomitized Carnian reef carbonates, which are situated adjacent to clay-rich basinal rocks, mottles of very finely to finely crystalline dolomite aggregates were interpreted to record the stages of progressive dolomitization in shallow and possibly in intermediate burial settings as a result of compaction-driven fluid flow (Haas et al. 2014a). The low $\delta^{18}O$ values, indicative of slightly elevated temperature, support this interpretation.

Geothermal convection

Pervasive dolomitization of the Middle Anisian platform carbonates (completely dolomitized version of the Tagyon Formation) can be explained by thermal convection (cf. Whitaker and Xiao 2010). However, this scenario is valid only for those areas where the platform conditions were restored after a relatively short drowning episode by the Late Anisian; therefore, the palaeogeographic conditions enabled the slope convection. In contrast, the other studied coeval isolated platform, which was buried by thick basin deposits with volcanic tuff interlayers, was not affected by this type of dolomitization, because its burial setting prevented effective sea water circulation (Haas et al. 2014b).

Those components of the latest Anisian to Ladinian platform succession which remained undolomitized or only partially dolomitized in the peritidal environment were subsequently replaced and cemented by medium and coarsely crystalline dolomite during burial at a temperature of ca 60–80 °C. An open half-cell thermal convection system and formation fluid flow, channelled along faults, may provide an adequate interpretation for this regional-scale intermediate burial dolomitization (Hips et al. 2015, 2016).

Fault-related dolomitization

Deeply penetrating fault zones were formed in the Lower Triassic formations, which reached the intermediate burial realm

at the time of opening of the Neotethys Ocean during the Middle Anisian to Ladinian. The ferroan carbonates, together with the barite sulphide mineral association found in the Lower Triassic rocks, suggest an influx of metal-transporting fluids. The underlying evaporite and red sandstone successions could have provided the brines and the metal supply for the mineralization. The ascending fluid reacted with the wall rocks and became acidic and reducing (cf. Dill 2010). This resulted in both the replacement of the remaining calcite and partial recrystallization of the earlier-formed dolomite by ferroan dolomite–ankerite. The effect of the ascending high-temperature fluid is supported by the negatively shifted $\delta^{18}O$ values. The associated paragenesis (i.e. ferroan carbonates and barite sulphide minerals) implies an exotic dolomitizing parent fluid enriched in certain metals.

The Middle Triassic and the early Late Triassic platform carbonates reached the intermediate–deep burial realm in the Jurassic. In the course of extensional tectonics, rock-buffered fracture-filling dolomite cements were formed at elevated temperature.

In the case of the Carnian–Norian slope and basinal formations, pervasive dolomitization is associated with syn-sedimentary normal faults (Hips et al. 2016). The maximum burial temperature of the succession was estimated from the thermal maturity data of the organic matter (Hetényi et al. 2004). Fluid inclusion homogenization temperature data (70 °C) compared to the ca. 50–60 °C maximum burial temperature suggests that the dolomitizing fluid was hydrothermal in origin. The warm fluid ascended along fault zones and cooled down through mixing with marine-derived pore fluid of the basinal deposits when it migrated away from the fault zones. This fluid flow mechanism differs remarkably from that of the well-known fault-related dolomitization models described from compressional settings (e.g. Oliver 1986; Machel et al. 2000; summary in Machel 2004). In the studied formations, the thermal gradient is considered as a potential driving force for the fluid flow.

Controlling factors

Based on inferences of these studies the palaeogeographic setting, sea level changes and climatic conditions can be considered as the main controlling factors of the near-surface and shallow burial dolomite formation. In the deeper burial settings the structural evolution and related fracturing and subsidence, and additionally the characteristics of the circulating fluids, may have been the decisive factors of the dolomite genesis.

Palaeogeographic setting

Near-surface dolomite formation took place in shallow ramp and platform environments in the TR. The continent-encroaching ramp setting determined the general sediment deposition pattern during the Early Triassic to early Middle Triassic interval. On the more than 100-km-wide shallow shelf, the hydrodynamic conditions determined the bottom topography and the depositional features of the sediments, whereas the amount of the terrestrial sediment input strongly influenced the composition of the sediments. Both the hydrodynamic conditions and the terrestrial input were controlled by sea level and climate.

In the middle part of the Middle Triassic, isolated carbonate platforms, characterized by flat tops and the lack of wave-resistant rims, came into existence. The building up of these platforms continued until the early Carnian. As a result of this topography sea level oscillation led to subaerial exposure of the platform tops during low sea level periods and inundation during the periods of rising sea level.

In the late Carnian, the filling up of most of the previously formed intraplatform basins gave rise to the development of an extensive shallow platform (Haas and Budai 1995; Haas 2002). However, at the same time, extensional basins formed near the Neotethys margin leading to segmentation of the external belt (north-eastern part of the TR) (Haas et al. 1995, 2010). The shallow parts of the segmented platform margin were permanently covered by sea during the late Carnian–Norian. In contrast, depositional conditions in the wide and nearly flat internal platform belt sensitively changed according to the sea level oscillation, leading to ephemeral subaerial exposure episodes during sea level lowstands (Haas and Budai 1995).

Sea level oscillation

The Middle and Upper Triassic internal platform succession of the TR is made up of metre-scale, subaerial unconformity-bounded cycles, consisting of alternating supratidal, intertidal and shallow subtidal facies (Haas 1988, 2004; Balog et al. 1999; Haas and Budai 1999; Haas et al. 2014b, 2015). Detailed studies (Fődolomit Formation and Dachstein Limestone) provided substantial arguments for the orbitally driven allocyclic control of the cyclicity of the platform sediments (Balog et al. 1997; Haas 2004; Haas et al. 2015). However, joint controlling effects of the sea level changes and the autocyclic processes cannot be excluded. According to the analyses and calculations of Schwarzacher and Haas (1986) the elementary cycles reflect ca 20-ka precessional periodicity. The Middle Triassic cyclic successions might also be orbitally forced but there is no reliable evidence either for the allocyclic control or for the duration of the cycles.

The cyclic depositional process can be interpreted according to the following scenario (Haas 2004; Haas et al. 2015): metre-scale sea level fall resulted in subaerial exposure of large parts of the previously inundated platform.

After a short exposure period, rising sea level led to the development of peritidal conditions when microbial mat covered large parts of the extensive tidal flat. Further sea level rise led to the establishment of shallow subtidal environments over the area previously covered by the microbial mats. However, in many cases, only the subtidal deposits were preserved. Deceleration and cessation of sea level rise resulted in shallowing and re-appearance of tidal flat environments usually covered by microbial mats. The next sea level fall resulted in subaerial exposure and related denudation, truncation and pedogenic alteration of the deposits formed during the previous cycle.

Climate

In shallow marine, peritidal and coastal environments, the climate is a crucial controlling factor of sedimentation and of near-surface early diagenetic processes. Beside temperature, the annual precipitation and related evaporation rate are other important factors. The enhanced evaporation of the arid to semi-arid regions also favours dolomite nucleation (Read and Horbury 1993; Purser et al. 1994). Modern examples of the organogenic dolomite/protodolomite formation can be found in arid to semi-arid environments, such as Lagoa Vermelha, Brazil (Vasconcelos and McKenzie 1997; Spadafora et al. 2010), the Coorong region, Australia (Wright and Wacey 2005), and the Abu-Dhabi sabkha (Bontognali et al. 2010). Occurrence of modern peritidal–coastal dolomite in humid and subhumid areas is very limited (Shinn 1968, 1983; Steinen and Halley 1979) and the proportion of dolomite in the carbonate deposits is usually <5 % (Budd 1997). Under arid–semi-arid conditions, evaporation transforms the marine water to mesohaline or hypersaline waters in the supratidal zone. The salinity gradient drives the modified water downward and seaward; therefore the reflux process commonly results in pervasive dolomitization in near-surface setting, but it may reach more than 100 m in depth (Whitaker and Smart 1993).

In the Triassic, the studied region was located between 20° and 35° North palaeolatitude. In the subtropical belt, the temperature was permanently high and trade winds dominated the air-mass circulation, which resulted in low precipitation (Feist-Bruckhardt et al. 2008). However, the long arid to semi-arid periods were interrupted by more humid episodes (the early Olenekian Campil Event; Broglio Loriga et al. 1990), and the Carnian Pluvial Event; Simms and Ruffell 1989; Preto et al. 2010; Haas et al. 2012; Dal Corso et al. 2015). A long-term climate change began in the late Norian. A gradual increase of humidity led to the establishment of humid climate at the very end of the Norian (Kössen Event; Golebiowski 1990; Haas 2002; Berra et al. 2010; Haas et al. 2012).

Studies of the Upper Triassic platform carbonates revealed that although the recurring subaerial exposure plays a decisive role in the near-surface dolomite formation, it is not the major controlling factor. Since the sea-level-controlled unconformity-bounded cyclic facies pattern did not change significantly during this period, the upward decreasing grade of dolomitization most likely reflects the change in climate. The drier climate and the related higher evaporation rates during the late Carnian to late Norian favoured dolomite formation, whereas later the increasing humidity led to gradually decreasing intensity of the early dolomitization processes (Haas 1988; Iannace and Frisia 1994; Balog et al. 1999).

Structural evolution

Structural evolution plays multiple roles in dolomite genesis. The bottom topography of the depositional environments is mainly determined by tectonic processes, i.e. the position of the shallow marine ramps, platforms, slopes and basins. Since the physiographic setting is a crucial element of the palaeogeography, it is one of the most important controlling factors of the near-surface dolomite-forming processes. Moreover, tectonic processes control the subsidence rate of the depositional units, thereby influencing the evolutionary history of the shallow and deep marine depositional units. From the aspect of evaluation of the hydrological conditions of dolomitization, the evolution of the usually tectonically controlled platform foreslopes is of particular relevance. Subsidence history of the structural–depositional units controls the burial, and in turn, the physical and chemical parameters of the burial dolomite-forming processes.

Creation of fracture porosity and thereby opening of conduits of fluids are important consequences of the tectonic processes, as well. They are commonly accompanied by dissolution and creation of secondary porosity. Due to the rigidity of dolostones, fracturing is not limited to narrow fault zones but the tectonic events may lead to the creation of a widely extended microfracture network. The tectonically enhanced porosity and permeability may facilitate the precipitation of dolomite cement and replacive dolomitization under intermediate to deep burial conditions.

The post-Variscan structural evolution of the study area was affected by the complex history of the Tethys Ocean and the subsequent Alpine orogeny. During the Late Permian to early Middle Triassic the area belonged to the vast, uniformly subsiding passive Tethys margin. The onset of the opening of the western Neotethys Ocean basin in the Middle Anisian led to disintegration of the margins and to the development of a segmented topography with isolated platforms, several hundred metres deep basins, and slope connecting them in the area of the TR. Faults created

during this extensional tectonic regime may have been the conduits of fluids, which caused ferroan dolomitization and barite sulphide mineralization in Lower Triassic formations. Dolomitization of the Middle Anisian platform carbonates was mostly controlled by the differential subsidence of the fault-bounded blocks. This platform was located on a more intensely subsiding block, which was covered by tuffaceous basinal deposits, and was not affected by burial dolomitization. In contrast, the platform, which was situated on a moderately subsiding block and where shallow marine conditions were restored after a drowning episode, the entire carbonate succession was pervasively dolomitized. During the Carnian to Norian new extensional basins developed in the ocean-ward north-eastern part of the TR. The basin-bounding fault zones served as conduits for the dolomitizing fluids. The onset of rifting of the Alpine Tethys in the latest Norian led to the formation of extensional basins also on the south-western side of the TR. An extensional regime prevailed all over the study area in the Jurassic, which resulted in the fragmentation of the previously formed platform carbonates, and was also manifested in the formation of neptunian dykes. Precipitation of the latest dolomite cement phases in fractures and other secondary pores of the buried Triassic dolostones and dolomitic limestones can be associated with these tectonic events.

Summary and concluding remarks

Large masses of dolomite-bearing formations occur in the Transdanubian Range (NW Hungary), forming a part of a nearly continuous Upper Palaeozoic to Cenozoic succession. However, the dolomite-bearing formations formed mostly in shallow marine and subordinately in deeper basinal environments, are restricted to the Late Permian–Late Triassic interval.

All the studied rock bodies underwent multi-stage and polygenetic dolomitization with variable dolomite-forming processes. These processes occurred either in near-surface or in burial diagenetic settings.

The main stage of dolomite genesis of the studied shallow marine formations most commonly occurred in the near-surface diagenetic zone where percolation of evaporative, higher density seawater through the previously deposited carbonate sediments caused replacive dolomitization. Only a subordinate amount of near-surface replacive dolomite was formed in the tidal flat deposits of the Upper Anisian–Ladinian formation, whose formation can be attributed to circulation of dolomitizing fluids driven by tidal pumping.

A minor amount of dolomite formed via organogenic dolomite precipitation in microbial deposits or via pedogenic processes in the case of the shallow marine and/or peritidal platform carbonates. However, differentiation of these early dolomite phases is rather difficult due to subsequent stage(s) of replacive dolomitization.

In addition to the petrographic investigations, comparative analysis of the studied successions and interpretation of the dolomite-forming processes were based on fluid inclusion data (when available) and the stable O and C-isotope data, which were measured in all studied formations. In spite of analysing mostly bulk samples with the exception of certain cement phases, it was possible to draw the following inferences about the distribution of the stable isotope values presented in Fig. 6. The C-isotope values are within the range of the Triassic seawater with the exception of the more negative values of the Early Triassic samples. This negative shift likely reflects the global ecologic perturbation after the cataclysm at the Permian/Triassic boundary and/or a diagenetic overprint. The O isotope values reflect the combined effects of isotopic fractionation due to evaporation and different formation temperatures, in addition to the secular changes of the seawater O isotope values (chemostratigraphic signal). The dominantly positive values of the Carnian–Norian platform carbonates indicate dolomitization by refluxing brines. Taking into account their tectonic setting and textural features, the slightly negative values of the Middle Anisian platform dolostones are interpreted to represent thermal convection-driven seawater dolomitizing fluid. The even more negative O isotope values of the Carnian platform margin deposits may reflect compaction-driven seawater of somewhat elevated temperature as the dolomitizing agent.

Inferences of the current study suggest that along with the palaeogeographic setting, climate and sea level changes were the main controlling factors of the dolomite-forming processes in syndepositional and near-surface burial diagenetic realms. The lateral extent of near-surface dolomite genesis was determined by the extension of areas affected by episodic subaerial exposure events. Such areas could be found in internal platform and inner ramp depositional settings. The temporal extent of the near-surface dolomite formation was controlled by climatic conditions such as temperature and humidity.

Our studies in the TR revealed that the deposits formed in episodically exposed shallow marine environments were subjected to significant near-surface dolomitization only when hot and arid to semi-arid conditions prevailed. Under semi-humid climatic conditions in the Late Norian, only a minor amount of organogenic dolomite was formed in tidal flat microbial deposits. The near-surface dolomite genesis practically ceased under the humid climate of the latest Triassic.

With progressing burial the circulation of the dolomitizing fluid generally becomes restricted due to decreasing porosity and permeability. Accordingly, usually only a

minor amount of dolomite formed in the TR in the intermediate burial realm. However, in rare cases the major phase of dolomitization occurred either via compactional fluid flow or via thermal convection in the intermediate burial realm.

During the Triassic, simultaneously with burial, several phases of extensional tectonic movements took place in connection with the opening of the Neotethys. The related fault zones provided conduits for dolomitizing fluids. Fault-related dolomitization in previous studies was considered only in compressional tectonic regimes. A new variation of fault-related dolomitization was proposed for an extensional tectonic regime based on our studies in the TR. According to our interpretation, the dolomitizing fluid was expelled along a synsedimentary normal fault system from the detachment zone. The thermal gradient in this intermediate burial setting is considered the potential driving force for fluid circulation. Permeable beds channelled the fluid from the fault zone upward and outward, which led to partial dolomitization of the succession. Thus, dolomitization was not restricted to the close vicinity of the faults.

In the case of the dolomitization of carbonate platforms, the tectonically controlled palaeogeographic setting, the sea-level-controlled periodical subaerial exposures and the climatic conditions are the major controlling factors of the initial dolomite formation and the reflux dolomitization. Divergent dolomitization of coeval neighbouring platforms of similar depositional conditions, but with different post-depositional tectonic and burial histories, was pointed out.

Our interpretation of dolomite-forming processes may provide feasible explanation for the genesis of other Triassic dolostones formed along the passive margin of the Tethys Ocean under depositional and diagenetic conditions akin to those in the TR. Moreover, our inferences may also be relevant in the interpretation of ancient dolostones occurring in other regions and representing other periods of the Earth's history. The limited applicability of the principles of actualism for the interpretation of the origin of large dolostone formations enhances the importance of these results.

Acknowledgments The present study was supported by the Hungarian National Science Fund (OTKA) grant K 81296 (J. Haas). The authors are indebted to Henry Lieberman (Houston) for the linguistic correction of the paper. The comments and suggestions of the reviewers Prof. Brian Jones and Prof. Patrick Meister improved the manuscript considerably.

References

Abed RMM, Kohls K, Palinska KA, Golubic S (2010) Diversity and role of cyanobacteria and aerobic heterotrophic microorganisms in carbon cycling in arid cyanobacterial mats. In: Seckbach J, Oren A (eds) Microbial mats, modern and ancient microorganism in stratified systems. Cellular Origin, Life in Extreme Habitats and Astrobiology Series, vol 14. Elsevier, Amsterdam, pp 255–276

Adams JE, Rhodes ML (1960) Dolomitization by seepage refluxion. AAPG Bull 44:1912–1920

Allen MA, Goh F, Burns BP, Neilan BA (2009) Bacterial, archaeal and eukaryotic diversity of smooth and pustular microbial mat communities in the hypersaline lagoon of Shark Bay. Geobiology 7:82–96

Alonso-Zarza AM, Wright VP (2010) Calcretes. In: Alonso-Zarza AM, Tanner LH (eds) Carbonates in continental settings. Elsevier, Amsterdam, pp 225–267

Alonso-Zarza AM, Sanz ME, Calvo JP, Estévez P (1998) Calcified root cells in Miocene pedogenic carbonates of the Madrid Basin: evidence for the origin of Microcodium. Sediment Geol 16:81–97

Balog A, Haas J, Read JF, Coruh C (1997) Shallow marine record of orbitally forced cyclicity in a Late Triassic carbonate platform, Hungary. J Sediment Res 67:661–675

Balog A, Read JF, Haas J (1999) Climate-controlled early dolomite, Late Triassic cyclic platform carbonates, Hungary. J Sediment Res 69:267–282

Banner JL, Hanson GN (1990) Calculation of simultaneous isotopic and trace element variations during water–rock interaction with applications to carbonate diagenesis. Geochim Cosmochim Acta 54:3123–3137

Berra F, Jadoul F, Anelli A (2010) Environmental control on the end of the Dolomia Principale/Hauptdolomit depositional system in the central Alps: coupling sea-level and climate changes. Palaeogeogr Palaeoclimatol Palaeoecol 290:138–150

Blendinger W (1997) Dolomitization of the Dolomites (Triassic Northern Italy): pilot study. Neues Jahrb Geol Paläontol Abh 204:83–110

Bontognali TRR, Vasconcelos C, Warthmann RJ, Dupraz C, Bernasconi S, McKenzie JA (2008) Microbes produce nanobacteria-like structures, avoiding cell entombment. Geology 36:663–666

Bontognali TRR, Vasconcelos C, Warthmann RJ, Bernasconi SM, Dupraz C, Strohmenger CJ, McKenzie JA (2010) Dolomite formation within microbial mats in the coastal sabkha of Abu Dhabi (United Arab Emirates). Sedimentology 57:824–844

Broglio Loriga C, Góczán F, Haas J, Lenner K, Neri C, Oravecz-Scheffer A, Posenato R, Szabó I, Tóth-Makk Á (1990) The Lower Triassic sequences of the Dolomites (Italy) and Transdanubian mid-mountains (Hungary) and their correlation. Mem Sci Geol XLII:41–103

Budai T, Haas J (1997) Triassic sequence stratigraphy of the Balaton Highland (Hungary). Acta Geol Hung 40:307–335

Budai T, Vörös A (1992) Middle Triassic history of the Balaton Highland: extensional tectonics and basin evolution. Acta Geol Hung 35:237–250

Budai T, Gy Lelkes, Piros O (1993) Evolution of Middle Triassic shallow marine carbonates in the Balaton Highland (Hungary). Acta Geol Hung 36:145–165

Budd DA (1997) Cenozoic dolomites of carbonate islands: their attributes and origin. Earth Sci Rev 42:1–47

Carballo JD, Land LS, Miser DE (1987) Holocene dolomitization of supratidal sediments by active tidal pumping, Sugarloaf Key, Florida. J Sediment Petrol 57:153–165

Choquette PW, Hiatt EE (2008) Shallow-burial dolomite cement: a major component of many ancient sucrosic dolomites. Sedimentology 55:423–460

Corsetti FA, Baud A, Marenco PJ, Richoz S (2005) Summary of Early Triassic carbon isotope records. C R Palevol 4:473–486

Csontos L, Vörös A (2004) Mesozoic plate tectonic reconstruction of the Carpathian region. Palaeogeogr Palaeoclimatol Palaeoecol 210:1–56

Dal Corso J, Gianolla P, Robert J, Newton RJ, Franceschi M, Roghi G, Caggiati M, Raucsik B, Budai T, Haas J, Preto N (2015)

Carbon isotope records reveal synchronicity between carbon cycle perturbation and the "Carnian Pluvial Event" in the Tethys realm (Late Triassic). Glob Planet Change 127:79–90

De Zanche V, Gianolla P, Mietto P, Siorpaes Ch, Vail P (1993) Triassic sequence stratigraphy in the Dolomites (Italy). Mem Sci Geol 45:1–27

Défarge C, Trichet J, Jaunet A-M, Robert M, Tribble J, Sansone FJ (1996) Texture of microbial sediments revealed by cryo-scanning electron microscopy. J Sediment Res 66(5):935–947

Dill HG (2010) The "chessboard" classification scheme of mineral deposits: mineralogy and geology from aluminum to zirconium. Earth Sci Rev 100:1–420

Dupraz C, Vischer PT, Baumgartner LK, Reid P (2004) Microbe–mineral interactions: early carbonate precipitation in a hypersaline lake (Eleuthera Island, Bahamas). Sedimentology 51:745–765

Dupraz C, Reid PR, Braissant O, Decho A, Norman RS, Visscher PT (2009) Processes of carbonate precipitation in modern microbial mats. Earth Sci Rev 96:141–162

Elrick M, Read JF (1991) Cyclic ramp to basin carbonate deposits. Lower Mississippian, Wyoming and Montana: a combined field and computer modelling study. J Sediment Res 61:1194–1224

Esteban M, Budai T, Juhász E, Lapointe PH (2009) Alteration of Triassic carbonates in the Buda Mountains—a hydrothermal model. Cent Eur Geol 52:1–29

Feist-Bruckhardt S, Götz AE, Szulc J, Borkhataria R, Geluk M, Haas J, Hornung J, Jordan P, Kempf O, Michalik J, Nawrocki J, Reinhardt L, Ricken W, Röhling H, Rüffer T, Török Á, Zühlke R (2008) Triassic. In: McCann T (ed) The geology of Central Europe. Geological Society, London, pp 750–821

Fischer AG (1964) The Lofer cyclothems of the Alpine Triassic. Kans Geol Surv Bull 169:107–149

Fischer AG (1991) Orbital cyclicity in Mesozoic strata. In: Einslele G, Ricken W, Seilacher A (eds) Cycles and events in stratigraphy. Springer, Berlin, Heidelberg, New York, pp 45–62

Fodor L, Koroknai B, Balogh K, Dunkl I, Horváth P (2003) A Dunántúli-középhegységi-egység (Bakony) takarós helyzete szlovéniai szerkezeti-geokronológiai adatok alapján (Nappe position of the Transdanubian Range Unit (Bakony) based on new structural and geochronological data from NE Slovenia). Földt Közlöny 133:535–546

Frisia S (1994) Mechanisms of complete dolomitization in a carbonate shelf: Comparison between the Norian Dolomia Principale (Italy) and the Holocene of Abu Dhabi Sabkha. In: Purser BH, Tucker ME, Zenger DH (eds) Dolomites. Blackwell, Oxford, London, Edinburgh, Boston, Melbourne, Paris, Berlin, Vienna, IAS Special Publications, pp 55–74

Gaetani M, Fois E, Jadoul F, Nicora A (1981) Nature and evolution of Middle Triassic carbonate buildups in the Dolomites (Italy). Mar Geol 44:25–57

Gawlick HJ (2000) Paläogeographie der Ober-Trias Karbonatplattform in den Nördlichen Kalkalpen. Mitt Ges Geol Bergbaustud Österr 44:45–95

Gawthorpe RL (1987) Burial dolomitization and porosity development in a mixed carbonate—clastic sequence: an example from the Bowland Basin, northern England. Sedimentology 34:533–558

Gianolla P, De Zanche V, Mietto P (1998) Triassic sequence stratigraphy in the Southern Alps (Northern Italy): definition of sequences and basin evolution. In: de Graciansky PC, Hardenbol J, Jacquin T, Vail PR (eds) Mesozoic and Cenozoic Sequence Stratigraphy of European Basins, SEPM Special Publications, vol 60, pp 719–747

Goldstein RH, James Reynolds T (1994) Systematics of fluid inclusions in diagenetic minerals. SEPM Short Course 31, SEPM, Tulsa

Golebiowski R (1990) The Alpine Kössen formation, a key for European topmost Triassic correlation. Albertiana 8:25–35

Gregg JM, Howard SA, Mazzullo SJ (1992) Early diagenetic recrystallization of Holocene (<3000 years old) peritidal Dolomites, Ambergris Cay, Belize. Sedimentology 39:143–160

Gregg JM, Bish DL, Kaczmarek SE, Machel HG (2015) Mineralogy, nucleation and growth of dolomite in the laboratory and sedimentary environment: a review. Sedimentology 62:1749–1769

Győri O, Poros Z, Mindszenty A, Molnár F, Fodor L, Szabó R (2011) Budai-hegységi paleogén karbonátos kőzetek diagenezistörténete (diagenetic history of the Palaeogene carbonates, Buda Hills, Hungary). Földt Közlöny 141(4):341–361

Haas J (1988) Upper Triassic carbonate platform evolution in the Transdanubian mid-mountains. Acta Geol Hung 31:299–312

Haas J (1994) Carnian basin evolution in the Transdanubian Central Range, Hungary. Zentralblatt Geol Paläontol Teil 1(H.11/12):1233–1252

Haas J (1995) Upper Triassic platform carbonates in the Northern Bakony Mts. Földt Közlöny 125:27–64

Haas J (2002) Origin and evolution of Late Triassic backplatform and intraplatform basins in the Transdanubian Range, Hungary. Geol Carpath 53:159–178

Haas J (2004) Characteristics of perididdal facies and evidences for subaerial exposures in Dachstein-type cyclic platform carbonates in the Transdanubian Range, Hungary. Facies 50:263–286

Haas J (2012) Geology of Hungary. Springer, Heidelberg

Haas J, Budai T (1995) Triassic facies zones in the Transdanubian Range. Riv Ital Paleontol Stratigr 101:249–266

Haas J, Budai T (1999) Triassic sequence stratigraphy of the Transdanubian Range, Hungary. Geol Carpath 50(6):459–475

Haas J, Demény A (2002) Early dolomitisation of Late Triassic platform carbonates in the Transdanubian Range (Hungary). Sediment Geol 151:225–242

Haas J, Tóth-Makk Á, Góczán F, Oravecz-Scheffer A, Oravecz J, Szabó I (1988) Lower Triassic key section in the Transdanubian mid mountains. Ann Inst Geol Publ Hung 65(2):131–173

Haas J, Császár G, Kovács S, Vörös A (1990) Evolution of the western part of the Tethys as reflected by the geological formations of Hungary. Acta Geod Geoph Mont Hung 25:325–344

Haas J, Kovács S, Krystyn L, Lein R (1995) Significance of Late Permian-Triassic facies zones in terrane reconstructions in the Alpine North Pannonian domain. Tectonophysics 242:19–40

Haas J, Tardi-Filácz E, Oravecz-Scheffer A, Góczán F, Dosztály L (1997) Stratigraphy and sedimentology of an Upper Triassic toe-of-slope and basin succession at Csővár-1, North Hungary. Acta Geol Hung 40(2):111–177

Haas J, Korpás L, Török Á, Dosztály L, Góczán F, Hámor-Vidó M, Oravecz-Scheffer, Tardi-Filácz E (2000) Felső-triász medence- és lejtőfáciesek a Budai-hegységben—a Vérhalom téri fúrás vizsgálatának tükrében (Upper Triassic basin and slope facies in the Buda Mts.—based on study of core drilling Vérhalom tér, Budapest). Földt Közlöny 130(3):371–421

Haas J, Götz AE, Pálfy J (2010) Late Triassic to Early Jurassic paleogeography and eustatic history in the NW Tethyan realm: new insights from sedimentary and organic facies of the Csővár Basin (Hungary). Palaeogeogr Palaeoclimatol Palaeoecol 291:456–468

Haas J, Budai T, Raucsik B (2012) Climatic controls on sedimentary environments in the Triassic of the Transdanubian Range (Western Hungary). Palaeogeogr Palaeoclimatol Palaeoecol 353–355:31–44

Haas J, Budai T, Győri O, Kele S (2014a) Multiphase partial and selective dolomitization of Carnian reef limestone (Transdanubian Range, Hungary). Sedimentology 61:836–859

Haas J, Budai T, Győri O, Kele S (2014b) Similarities and differences in the dolomitization history of two coeval Middle Triassic carbonate platforms, Balaton Highland, Hungary. Facies 60(2):581–602

Haas J, Budai T, Demény A (2014c) Partial dolomitization of foreslope and toe-of-slope facies of a Carnian carbonate platform, Transdanubian Range, Hungary. Cent Eur Geol 57(1):1–19

Haas J, Lukoczki G, Budai T, Demény A (2015) Genesis of Late Triassic peritidal dolomites in the Transdanubian Range, Hungary. Facies. doi:10.1007/s10347-015-0435-7

Hardie LA, Bosellini A, Goldhammer RK (1986) Repeated subaerial exposure of subtidal carbonate platforms, Triassic, Northern Italy: evidence for high-frequency sea level oscillation on a 104 year scale. Paleoceanography 1:447–457

Henrich R, Zankl H (1986) Diagenesis of Upper Triassic Wetterstein reefs of the Bavarian Alps. In: Schroeder JH, Purser BH (eds) Reef diagenesis. Springer, Berlin, pp 245–268

Hetényi M, Cs Sajgó, Vető I, Brukner-Wein A, Szántó Z (2004) Organic matter in a low productivity anoxic intraplatform basin in the Triassic Tethys. Org Geochem 35:1201–1219

Hips K, Haas J, Z Poros, Kele S, Budai T (2015) Dolomitization of Triassic microbial mat deposits (Hungary): origin of microcrystalline dolomite. Sediment Geol 318:113–129

Hips K, Haas J, Győri O (2016) Hydrothermal dolomitization of basinal deposits controlled by a synsedimentary fault system in Triassic extensional setting, Hungary. Int J Earth Sci 105:1215–1231

Iannace A, Frisia S (1994) Changing dolomitization styles from Norian to Rhaetian in the Southern Tethys realm. In: Purser BH, Tucker ME, Zenger DH (eds) Dolomites. IAS, London, pp 75–89

Illing LV (1959) Deposition and diagenesis of some upper Paleozoic carbonate sediments in western Canada. Fifth World Petroleum Congress, New York, pp 23–52

Joachimski MM, Lai X, Shen S, Jiang H, Luo G, Chen B, Sun Y (2012) Climatic warming in the latest Permian and the Permian-Triassic mass extinction. Geology 40:195–198

Jones GD, Xiao Y (2005) Dolomitization, anhydrite cementation, and porosity evolution in a reflux system: insight from reactive transport models. AAPG Bull 89:577–601

Kendall AC (1985) Radiaxial-fibrous calcite: a reappraisal. In: Schneidermann N, Harris PM (eds) Carbonate cements, vol 36. SEPM Special Publication, Tulsa, OK, pp 59–77

Korte C, Kozur HW, Veizer J (2005) $\delta^{13}C$ and $\delta^{18}O$ values of Triassic brachiopods and carbonate rocks as proxies for coeval seawater and palaeotemperature. Palaeogeogr Palaeoclimatol Palaeoecol 226:287–306

Land LS (1983) The application of stable isotopes to studies of the origin of dolomite and to problems of diagenesis of clastic sediments. In: Arthur MA, Anderson TF, Kaplan IR, Veizer J, Land LS (eds) Stable isotopes in sedimentary geology. Society of Sedimentary Geology, Tulsa, pp 4.1–4.22

Land LS (1985) The origin of massive dolomite. J Geol Educ 33:112–125

Leutloff AH, Meyers WJ (1984) Regional distribution of microdolomite inclusions in Mississippian echinoderms from southwest New Mexico. J Sediment Petrol 54:432–446

Lobitzer H, Mandl GW, Mazzullo SJ, Mello J (1990) Comparative study of Wetterstein carbonate platforms of the easternmost Northern Calcareous Alps and West Carpathian mountains: preliminary results. In: Minarikova D, Lobitzer H (eds) Thirty years of geological cooperation between Austria and Czechoslovakia. Federal Geological Survey, Vienna, Geological Survey, Prague, pp 136–158

Lohmann KC, Meyers WJ (1977) Microdolomite inclusions in cloudy prismatic calcites? A proposed criterion for formerly high magnesium calcite. J Sediment Petrol 47:1078–1088

Lucia FJ, Major RP (1994) Porosity evolution through hypersaline reflux dolomitization. In: Purser BH, Tucker ME, Zenger DH (eds) Dolomites. Blackwell, Oxford, London, Edinburgh, Boston, Melbourne, Paris, Vienna, IAS Special Publication, pp 325–341

Machel HG (2004) Concepts and models of dolomitization: a critical reappraisal. In: Braithwaite C, Rizzi G, Darke G (eds) The geometry and petrogenesis of dolomite hydrocarbon reservoirs. Geol Soc Spec Publ, London, pp 7–63

Machel HG, Anderson JH (1989) Pervasive subsurface dolomitization of the Nisku Formation in central Alberta. J Sediment Petrol 59:891–911

Machel HG, Cavell PA, Buschkuehle BE, Michael K (2000) Tectonically induced fluid flow in Devonian Carbonate aquifers of the Western Danada Sedimentary Basin. J Geochem Explor 50:332–338

Mandl GW (2000) The Alpine sector of the Tethyan shelf—examples of Triassic to Jurassic sedimentation and deformation from the Northern Calcareous Alps. Mitt Gesellsch Geol Bergb Öst 92:61–77

Mazzullo SJ (2000) Organogenic dolomitization in peritidal to deep-sea sediments. J Sediment Res 70:10–23

Mazzullo SJ, Reid AM, Gregg JM (1987) Dolomitization of Holocene Mg-calcite supratidal deposits, Ambergis Cay, Belize. Geol Soc Am Bull 89:224–231

Meister P, McKenzie JA, Bernasconi SM, Brack P (2013) Dolomite formation in the shallow seas of the Alpine Triassic. Sedimentology 60:270–291

Monty CLV (1967) Distribution and structure of recent stromatolitic algal mats, Eastern Andros Island, Bahamas. Ann Soc Geol Belg 90:55–100

Monty CLV (1981) Spongiostromate versus Porostromate stromatolites and oncolites. In: Monty CLV (ed) Phanerozoic stromatolites. Springer, Berlin, pp 1–4

Morrow DW (1982) Dolomite—part 2: dolomitization models and ancient dolostones. Geosci Can 9:95–107

Narkiewicz M, Retallack GJ (2014) Dolomitic paleosols in the lagoonal tetrapod track-bearing succession of the Holy Cross Mountains (Middle Devonian, Poland). Sediment Geol 299:74–87

Oliver J (1986) Fluids expelled tectonically from orogenic belts: their role in hydrocarbon migration and other geologic phenomena. Geology 14:99–102

Poros Z (2011) Fluid migration and porosity evolution in the Buda Hills, Hungary—selected examples from Triassic and Paleogene carbonate rocks. PhD dissertation Thesis, Eötvös University, Budapest, 141 pp

Poros Z, Mindszenty A, Molnár F, Pironon J, Győri O, Ronchi P, Szekeres Z (2012) Imprints of hydrocarbon-bearing basinal fluids on a karst system: mineralogical and fluid inclusion studies from the Buda Hills, Hungary. Int J Earth Sci 101:429–452

Poros Z, Machel HG, Mindszenty A, Molnár F (2013) Cryogenic powderization of Triassic dolostones in the Buda Hills, Hungary. Int J Earth Sci 102:1513–1539

Preto N, Kustatscher E, Wignall PB (2010) Triassic climates-state of the art and perspectives. Palaeogeogr Palaeoclimatol Palaeoecol 290:1–10

Purser BH, Tucker ME, Zenger DH (1994) Problems, progress and future research concerning dolomites and dolomitization. In: Purser BH, Tucker ME, Zenger DH (eds) Dolomites. Blackwell, Oxford, London, Edinburgh, Boston, Melbourne, Paris, Berlin, Vienna, IAS Special Publication, pp 3–20

Read JF, Horbury AD (1993) Eustatic and tectonic controls on porosity evolution beneath the sequence-bounding unconformities and parasequence disconformities on carbonate platforms. In: Horbury AD, Robinson AG (eds) Diagenesis and Basin development. AAPG Stud Geol, Tulsa, pp 155–197

Roberts JA, Kenward PA, Fowle DA, Goldstein RH, González LA, Moore DS (2013) Surface chemistry allows for abiotic

precipitation of dolomite at low temperature. Proc Natl Acad Sci USA 110(36):14540–14545
Rosenbaum J, Sheppard SMF (1986) An isotopic study of siderites, dolomites and ankerites at high temperatures. Geochim Cosmochim Acta 50:1147–1150
Sánchez-Román M, Vasconcelos C, Schmid T, Dittrich M, McKenzie JA, Zenobi R, Rivadeneyra MA (2008) Aerobic microbial dolomite at the nanometer scale: implications for the geologic record. Geology 36:879–882
Schwarzacher WJ, Haas J (1986) Comparative statistical analysis of some Hungarian and Austrian Upper Triassic peritidal carbonate sequences. Acta Geol Hung 29:175–196
Shinn E (1968) Selective dolomitization of recent sedimentary structures. J Sediment Petrol 38:612–616
Shinn E (1983) Tidal flat environment. In: Scholle PA, Bebout DG, Moore CH (eds) Carbonate depositional environments. AAPG Mem, Tulsa, pp 171–210
Simms MA (1984) Dolomitization by groundwater flow systems in carbonate platforms. Gulf Coast Assoc Geol Sci Trans 24:411–420
Simms MJ, Ruffell AH (1989) Synchroneity of climatic change and extinctions in the Late Triassic. Geology 17:265–268
Spadafora A, Perri E, McKenzie JA, Vasconcelos C (2010) Microbial biomineralization processes forming modern Ca: Mg carbonate stromatolites. Sedimentology 57:27–40
Spötl C, Burns SJ (1991) Formation of ^{18}O-depleted dolomite within a marine evaporitic sequence, Triassic Reichenhall Formation, Austria. Sedimentology 38:1041–1057
Spötl C, Pitman JK (1998) Saddle (baroque dolomite) in carbonates and sandstones: a reappraisal of a burial diagenetic concept. IAS Spec Publ 26:437–460
Spötl C, Vennemann TW (2003) Continuous-flow isotope ratio mass spectrometric analysis of carbonate minerals. Rapid Commun Mass Spectrom 17:1004–1006
Steinen RP, Halley RB (1979) Ground water observations on small carbonate islands of southern Florida. In: Halley RB (ed) Guidebook to sedimentation for the Dry Tortugas. GSA, Boulder, pp 82–89
Sun Y, Joachimski MM, Wignall PB, Yan C, Chen Y, Jiang H, Wang L, Lai X (2012) Lethally hot temperatures during the early Triassic greenhouse. Science 338:366–370
Tari G, Horváth F (2010) Eo-Alpine evolution of the Transdanubian Range in the Alpine nappe system of the Eastern Alps: revival of a 15 years tectonic model. Földt Közlöny 140:483–510
Teal CS, Mazzulo SJ, Bischoff WD (2000) Dolomitization of Holocene shallow marine deposits mediated by sulphate reduction and methanogenesis in normal-salinity seawater, Northern Belize. J Sediment Res 70(3):649–663
Vasconcelos C, McKenzie JA (1997) Microbial mediation of modern dolomite precipitation and diagenesis under anoxic conditions, Lagoa Vermelha, Rio de Janero, Brazil. J Sediment Res 67:378–390
Vasconcelos C, McKenzie JA, Bernasconi S, Grujic D, Tien AJ (1995) Microbial mediation as a possible mechanism for natural dolomite formation at low temperatures. Nature 377:220–222
Wenk HR, Hu M, Frisia S (1993) Partially disordered dolomite: microstructural characterization of Abu Dhabi sabkha carbonates. Am Mineral 78(7–8):769–774
Whitaker FF, Smart PL (1993) Circulation of saline groundwaters in carbonate platforms: a review and case study from the Bahamas. In: Horbury AD, Robinson AG (eds) Diagenesis and Basin development. AAPG Stud Geol, Tulsa, pp 113–132
Whitaker FF, Xiao Y (2010) Reactive transport modelling of early burial dolomitization of carbonate platforms by geothermal convection. AAPG Bull 94:889–917
Wright VP (1990) Carbonate sediments and limestones: constituents. In: Tucker ME, Wright VP (eds) Carbonate sedimentology. Blackwell, Oxford, pp 1–27
Wright VP (1994) Paleosols in shallow marine carbonate sequences. Earth Sci Rev 35:367–395
Wright DT (2000) Benthic microbial communities and dolomite formation in marine and lacustrine environments—new dolomite model. In: Glenn CR, Pevot-Lucas L, Lucas J (eds) Marine authigenesis: from global to microbial. SEPM Special Publication, Tulsa, pp 7–20
Wright VP (2007) Calcrete. In: Nash DJ, McLaren SJ (eds) Geochemical sediments and landscapes. Blackwell Publishing Ltd, Oxford, pp 10–47
Wright VP, Tucker ME (1991) Calcretes. Blackwell, Oxford
Wright DT, Wacey D (2005) Precipitation of dolomite using sulphate-reducing bacteria from the Coorong Region, South Australia: significance and implication. Sedimentology 52:987–1008
Zhang F, Xu H, Konishi H, Kemp JM, Roden EE, Shen Z (2012a) Dissolved sulphide-catalyzed precipitation of disordered dolomite: implication for the formation mechanism of sedimentary dolomite. Geochimi Cosmochim Acta 97:148–165
Zhang F, Xu H, Konishi H, Shelobolina ES, Roden EE (2012b) Polysaccharide-catalyzed nucleation and growth of disordered dolomite: a potential precursor of sedimentary dolomite. Am Mineral 97:556–567
Zhang F, Xu H, Shelobolina ES, Konishi H, Converse B, Shen Z, Roden EE (2015) The catalytic effect of bound extracellular polymeric substances by anaerobic microorganisms on Ca–Mg carbonate precipitation: implications for the “dolomite Problem”. Am Mineral 100:483–494